People's democratic republic of Algeria

Ministry of higher education and scientific research

Order number :

Serial number :

University of Echahid Hamma Lakhdar - El Oued

Faculty of exact sciences

Department of physics

A graduation thesis submitted to obtain a degree of

# Academic Master

Field: mater sciences

Specialty: medical physics

Prepared by: DRISS Safia Belkis

Subject:

# Quantum chemical analysis of caffeic acid as a biological antioxidant and potential radioprotector

Defended on: 18/06/2026

Before the examination committee composed of:

| | | | |
|---|---|---|---|
| MIMOUNI Mourad | Assoc.prof | President | El Oued University |
| GHERAISSA Nadjet | Asst .Prof | Examiner | El Oued University |
| ZEROUAL Soria | Professor | Supervisor | El Oued University |

Laboratory of Exploitation and Valorization of Saharan Energy Resources (LEVRES)

Academic Year: 2025/ 2026

# Thanks and appreciation

{ وَآخِرُ دَعْوَاهُمْ أَنِ الْحَمْدُ لِلَّهِ رَبِّ الْعَالَمِينَ }

**Praise be to God for this auspicious beginning and a fitting conclusion.**

**I am grateful for your immense favor and blessings upon me. Praise be to God for the strength, patience, and success. He granted me the ability to complete this work.**

**I would like to express my sincere gratitude and deep appreciation to my supervisor, Pr. ZEROUAL Soria, for her academic guidance, valuable advice, and continuous support and encouragement throughout the research and writing of this project.**

**My sincere thanks go to the president of the jury Dr.MIMOUNI Mourad for presiding over my thesis defense and to the examiner, Dr.Gheraissa Nadjet for evaluating this work and providing valuable comments.**

**I also extend my sincere thanks to Pr. Mahboub Mohammed Sadok, Director of the Laboratory for the Exploitation and Valorization of Saharan Energy Resources (LEVRES), for all the facilities he provided to us, as well as to the laboratory engineer, Guedda Othmane.**

**Special thanks to Dr.Touati Brahim Mohammed Said and Dr.Mimouni Mourad, who gave me the opportunity to study this specialty.**

**Finally, I offer my love and appreciation to everyone who showed me genuine support, praying for the well-being of all.**

**Safia Belkis**

# Dedication

**We embarked on our journeys only through His facilitation, we reached our ends only through His guidance, and we achieved our goals only through His grace.**

**So, praise be to God, with love, thanks, and gratitude. Praise be to God for the beginning and the end.**

**He who says, "I am ready for it," attains it. And I am ready for it, even if it refuses me against its will. I attain it and embrace great glory.**

***To the soul of my father, Lachouri:*** **Thanks to your kindness, sacrifices, and unconditional love, you instilled in me strength I never thought I possessed. You were my support, the one I always relied on, even in the most difficult times. You are my hero. Your memory is engraved in my heart with every breath, with every thought. This work is a testament to your legacy and all that you bequeathed to me and taught me. May your soul rest in peace, and may your love be my companion in every step of my life. Today, even though you're gone, I feel your presence every moment, and I'm certain you'll always be with me, guiding me and illuminating my path.**

***To my beloved mother, Noura,*** **the embodiment of quiet courage and boundless love, who, after losing my father, shouldered the responsibility of parenthood alone. You were my light in the darkest times and my strength when I was weak. You gave generously and loved unconditionally. This work is dedicated to your sacrifice, your kindness, and the remarkable strength you embody every day. May God protect you as you have protected me throughout my life.**

**To those who extended their hands in my time of weakness, to the best and purest of my days, to the candles that light my way and who have long awaited this moment to be proud of me, my sisters *Nassiba, Fatima, and Maria.***

**To my small family who accompanied me in times of hardship and were my support and strength: *my uncle, Okba, my aunt Sabah, Hanan, Dido, Anais, Amir and Warda***

**To everyone who was a help and support on this path... To my loyal maternal uncles ,friends and companions of many years,**

**To those who stood by me in times of hardship and crisis.**

**I dedicate this achievement and the fruit of my success, which I have always longed for. Today, I have completed and fulfilled its first fruits, thanks to God Almighty. Praise be to God for what He has bestowed upon me**

***Safia belkis***

## Summary of Contents

# Summary of Contents

# Summary of Contents

# Summary of figures

## Chapter one



## Chapter three

# Summary of tables

## Chapter one



## Chapter three

# Summary of tables

# List of symbols and abbreviations

| | |
|---|---|
| **CA** | **Caffeic acid** |
| **CAR** | **Caffeic acid radical** |
| **DFT** | **Density functional theory** |
| **ROS** | **Reactive oxygen species** |
| **HOMO** | **Highest occupied molecular orbital** |
| **LUMO** | **Lowest unoccupied molecular orbital** |
| **($OH^{\bullet}$)** | **Hydroxyl radical** |
| **($H^{\bullet}$)** | **Hydrogen radicals** |
| **($O_2^{-\bullet}$)** | **Superoxide anions** |
| **$H_2O$** | **Dihydrogen monoxide** |
| **$H_2O_2$** | **Hydrogen peroxide** |
| **DNA** | **Deoxyribonucleic acid** |
| **BDE** | **Bond dissociation enthalpy** |
| **MEP** | **Molecular electrostatic potential** |
| **LET** | **Linear energy transfer** |
| **PCM** | **Polarizable continuum model** |
| **$\psi$** | **Wave function of the system** |
| **$E$** | **Total energy of the system** |
| **$\hat{H}$** | **Hamilton of the system** |
| **$T_e$** | **Kinetic energy of the electrons** |
| **$T_n$** | **Kinetic energy of the nuclei** |

# List of symbols

| | |
|---|---|
| $V_{ne}$ | Nucleus-electron attraction potential |
| $V_{ee}$ | Electron-electron repulsion potential |
| $V_{nn}$ | Nucleus-nucleus repulsion potential |
| $E_{[\rho]}$ | Total energy functional |
| $\rho\ (r)$ | Eelectron density at position |
| $V_{ext}\ (r)$ | External potential (Nuclei-electron interaction) |
| $F_{HK[\rho]}$ | Universal Hohenberg -kohn functional |
| $T_{[\rho]}$ | Kinetic energy of the electrons |
| $V_{[\rho]}$ | Electron-electron repulsion energy |
| $\Phi_i$ | Kohn-sham orbitals |
| $\varepsilon_i$ | Orbital energies |
| $V_{eff}\ (r)$ | Effective potential |
| $V_{xc}\ (r)$ | Exchange-correlation potential |
| IR | Infrared spectroscopy |

# GENERAL INTRODUCTION

# General Introduction

Medical physics is a fundamental discipline in modern healthcare, integrating physics principles with medicine to improve the diagnosis and treatment of diseases. It plays a crucial role in medical imaging modalities such as X-ray radiography, computed tomography (CT), magnetic resonance imaging (MRI), nuclear medicine, and in radiation therapy for cancer management. Among these applications, radiotherapy remains one of the most effective techniques for tumor control. However, the use of ionizing radiation inevitably exposes normal tissues surrounding the tumor to radiation, which may lead to undesirable biological effects [1].

When ionizing radiation interacts with biological matter, it deposits energy along its path, producing ionizations and excitations in water and biomolecules. Since the human body is mainly composed of water, radiation interaction results in the radiolysis of water and the generation of reactive oxygen species (ROS) such as hydroxyl radicals ($OH^{\bullet}$), superoxide anions ($O_2^{\bullet-}$), and hydrogen peroxide ($H_2O_2$). These reactive species are highly unstable and can attack essential cellular components including DNA, proteins, and lipids. DNA damage, such as single-strand breaks, double-strand breaks, and base modifications, is considered one of the most critical consequences of radiation exposure and is directly related to cell death, mutations, and long-term biological risks [2].

In radiotherapy, the objective is to deliver a high dose to tumor tissues while sparing surrounding healthy organs as much as possible. Nevertheless, radiation-induced oxidative stress remains a major limitation, leading to side effects such as inflammation, fibrosis, and functional impairment of normal tissues. From the perspective of medical physics, improving the therapeutic ratio between tumor control probability (TCP) and normal tissue complication probability (NTCP) is essential. One promising approach to achieve this balance is the use of radioprotective agents that selectively protect normal cells without reducing the effectiveness of radiation on tumor cells [3].

Radioprotectors are substances capable of reducing the biological damage produced by ionizing radiation. Their mechanisms of action include scavenging free radicals, donating electrons or hydrogen atoms, enhancing DNA repair, and stabilizing cellular membranes.

Classical synthetic radioprotectors often suffer from toxicity and limited clinical applicability. Therefore, there is growing interest in natural compounds with antioxidant activity, which are generally safer and more compatible with biological systems. Antioxidants reduce oxidative stress by neutralizing ROS and preventing chain reactions that damage biomolecules [4].

Caffeic acid is a naturally occurring phenolic compound widely distributed in coffee, fruits, vegetables, and olive oil. It is well known for its antioxidant, anti-inflammatory, and cytoprotective properties. The molecular structure of caffeic acid contains conjugated double bonds and hydroxyl functional groups that can easily donate electrons or hydrogen atoms to stabilize free radicals. This chemical behavior makes caffeic acid an interesting candidate as a biological radioprotector. In the context of medical physics, understanding how such a molecule interacts with radiation-induced ROS at the molecular level is essential for evaluating its potential application in radiotherapy and radiation protection [5].

Experimental investigation of radioprotective properties can be costly and time-consuming. For this reason, theoretical and computational approaches have become increasingly important.

Quantum chemistry provides a powerful framework to describe molecular systems based on the principles of quantum mechanics. Among the available methods, density functional theory (DFT) is one of the most widely used techniques for studying the electronic structure and reactivity of molecules. DFT allows the calculation of molecular orbitals, charge distribution, dipole moment, molecular electrostatic potential, and global reactivity descriptors, which are directly related to chemical and biological activity [6].

In particular, the analysis of the highest occupied molecular orbital (HOMO) and the lowest unoccupied molecular orbital (LUMO) give valuable information about the ability of a molecule to donate or accept electrons; A high HOMO energy indicates good electron-donating capacity, which is closely associated with antioxidant behavior.

The HOMO–LUMO energy gap is related to chemical reactivity and stability: a smaller gap generally corresponds to higher reactivity toward free radicals. Moreover, molecular electrostatic potential (MEP) maps help identify electrophilic and nucleophilic regions of the molecule, indicating the preferred sites for interaction with ROS. Dipole moment and charge distribution further describe how the molecule behaves in a biological environment [7].

Within the framework of medical physics, quantum chemical modeling serves as a bridge between fundamental electronic properties and macroscopic biological protection. By elucidating the intrinsic reactivity of caffeic acid at the sub-atomic level, this approach provides a predictive roadmap to understand how molecular stability and electron-donating efficiency translate into clinical radioprotective potential, ultimately aiming to enhance the safety and efficacy of modern radiotherapy protocols.

This study was divided into:

**Chapter One:** provides a comprehensive theoretical foundation for the study. It begins by analyzing the fundamentals of medical physics and the nature of ionizing radiation. The discussion then focuses on the mechanisms of radiation interaction with biological matter, specifically the radioactive decay of water and the subsequent production of reactive oxygen species (ROS). Furthermore, the chapter explores the role of caffeic acid as a natural radioprotective agent, emphasizing its molecular structure and its ability to neutralize oxidative stress.

**Chapter two**: In this chapter the computational framework is established by introducing density functional theory (DFT) and quantum indices (such as HOMO/LUMO orbitals and the energy gap) used to evaluate molecule reactivity at the subatomic level.

**Chapter three:** focuses on the presentation and discussion of the numerical results obtained from the quantum calculations. It begins with the geometric optimization of the caffeic acid molecule, followed by an analysis of its chemical reactivity through frontier molecular orbitals (HOMO-LUMO) and molecular electrostatic potential (MEP) maps.

The chapter also evaluates the antioxidant activity by calculating the bond dissociation enthalpy (BDE) and ($\Delta E$). Finally, the study concludes with a detailed spectroscopic analysis, where the theoretical FT-IR and Raman spectra are compared with experimental data to validate the molecular model. by evaluating the antioxidant activity of caffeic acid and the molecule's capacity to scavenge free radicals.

# References

[1] J. G. Webster, and J. D. Bronzino, "Medical instrumentation: Application and Design", 4th ed, Wiley, (2015).

[2] E. J. Hall, and A. J. Giaccia, "Radiobiology for the Radiologist", 8th ed, Lippincott Williams & Wilkins, (2018).

[3] F. M. Khan, "The Physics of Radiation Therapy", 5th ed, Lippincott Williams & Wilkins, (2014).

[4] M. C. Joiner, and A. J. van der Kogel, "Basic Clinical Radiobiology", 5th ed, CRC Press, (2018).

[5] İ. Gülçin, "Antioxidant activity of caffeic acid (3, 4-dihydroxycinnamic acid)", Toxicology, 217, N°2-3, 213–220, (2006).

[6] W. Koch, and M. C. Holthausen, "A Chemist's Guide to Density Functional Theory", 2nd ed, Wiley-VCH, (2015).

[7] M. S. Abdel-Mottaleb, et al., "DFT Studies of Caffeic Acid Antioxidant: Molecular Orbitals and Composite Reactivity Maps", Journal of Chemistry, 2016, 1–10, (2016).

# CHAPTER ONE:

# Medical physics, antioxidants and radioprotectors

# I.1. Introduction

The integration of physical principles into the medical realm has fundamentally redefined the landscape of modern oncology and diagnostic medicine.

At the core of this integration lies Medical Physics, a discipline that harmonizes complex physical theories with clinical requirements to optimize cancer treatment strategies.

The efficacy of radiotherapy, while profound in its ability to neutralize malignant cells, is intrinsically linked to the intricate ways in which ionizing radiation interacts with biological matter; These interactions initiate a series of multi-scale events ranging from sub-atomic energy depositions to macroscopic tissue responses.

Central to these processes is the phenomenon of water radiolysis and the subsequent generation of reactive oxygen species (ROS), which act as the primary mediators of both therapeutic success and collateral damage. This chapter aims to establish a comprehensive theoretical framework, exploring the physical nature of radiation, the biochemical pathways of oxidative stress, and the strategic role of antioxidants, specifically Caffeic acid, in mitigating radiation-induced cellular injury.

# I.2. Medical physics and ionizing radiation

## I.2.1. Foundations of medical physics in clinical practice

Medical physics serves as a critical bridge between theoretical physical principles and clinical applications, primarily focusing on enhancing diagnostic precision and therapeutic efficacy. Within the oncology sector, this discipline is indispensable for ensuring the safety and accuracy of treatments. This involves rigorous dose calculations, stringent quality assurance protocols, and the implementation of robust radiation protection strategies, all aimed at optimizing patient outcomes while maintaining high standards of clinical safety [1].

## I.2.2. Classification and nature of ionizing radiation

At its core, ionizing radiation is defined by its capacity to deposit sufficient energy into a medium to liberate electrons from atomic structures, thereby creating ion pairs. This radiation is broadly categorized based on its physical properties into electromagnetic forms, such as X-rays and gamma rays, and particulate forms, including electrons, protons, alpha particles, and neutrons. From a mechanistic perspective, these radiations are further distinguished by their mode of interaction: charged particles are considered directly ionizing as they interact immediately with atomic nuclei and electrons, whereas photons (X-rays and gamma rays) are indirectly ionizing, as they must first release secondary charged particles to initiate biological damage [2].

## I.2.3. Physical determinants of biological impact

The severity of radiation-induced effects is fundamentally governed by specific physical parameters that characterize the energy deposition process. The absorbed dose, measured in Grays (Gy), quantifies the energy distributed per unit mass, yet it does not fully account for the biological outcome.
The linear energy transfer (LET) is a crucial factor in this context, as it describes the energy deposition density along the radiation track. Compared to low-LET radiation, high-LET particles produce much denser ionization paths, which significantly enhances their relative biological effectiveness and leads to more complex cellular damage [3].

The primary objective of radiotherapy is the targeted destruction of malignant cells through the induction of lethal genomic lesions. This is achieved via two primary pathways: the direct ionization of the DNA molecule or, more commonly, an indirect process facilitated by the radiolysis of water, which generates highly reactive oxygen species (ROS). The clinical success of these treatments hinges on the therapeutic ratio, that is a delicate balance designed to maximize the probability of tumor control (TCP) while concurrently reducing the normal tissue complication probability (NTCP) [4].

## I.3. Interaction of radiation with biological matter:

The interaction between ionizing radiation and biological systems initiates through a sequence of distinct yet interconnected stages, beginning with the physical stage. Occurring almost instantaneously (within $10^{-15}$ to $10^{-12}$ seconds), this phase is characterized by the deposition of radiant energy, leading to the fundamental processes of ionization and excitation. These events culminate in the emergence of primary ions and free electrons, the density of which is strictly dictated by the radiation's linear energy transfer (LET). While electromagnetic radiations like X-rays generate sparsely distributed events (low-LET), particulate radiations such as alpha particles create highly concentrated ionization tracks, significantly increasing the probability of direct molecular hits [2].

Transitioning into the Chemical Stage ($10^{-12}$ to $10^{-6}$ seconds), the previously formed ions undergo rapid transformations to produce highly reactive chemical species. Given the aqueous nature of the cellular environment, the radiolysis of water molecules becomes the dominant pathway, yielding a variety of reactive oxygen species (ROS) including hydroxyl radicals ($OH^{\bullet}$) hydrogen radicals ($H^{\bullet}$), and superoxide anions ($O_2^{-\cdot}$). These species, though short-lived, are capable of diffusing short distances to attack vital macromolecules, thereby translating physical energy into chemical damage across DNA, protein, and lipid structures [4].

The biological stage represents the longest phase, extending from seconds to several hours post-irradiation. This period is defined by the manifestation of structural damage to the genome, manifesting as base modifications and single or double-strand breaks. The cell's fate is determined by its intrinsic enzymatic repair capacity; successful repair maintains cellular viability, whereas irreparable lesions often trigger programmed cell death (apoptosis) or mitotic failure. This biological outcome is not uniform but is influenced by the cellular microenvironment, including the proliferation rate and the metabolic state of the tissue [4].

The extent of biological degradation is modulated by several key factors that define the "Radiosensitivity" of the target. Beyond the physical influence of LET, the oxygen effect plays a paramount role; well-oxygenated environments exacerbate damage by stabilizing ROS-induced lesions. Furthermore, according to classical radiobiological laws, cells that are rapidly dividing or in specific

phases of the cell cycle exhibit heightened susceptibility to genomic disruption. Mastery of these interactive variables is the cornerstone of modern radiotherapy, enabling clinicians to refine tumor-killing efficiency while preserving the integrity of adjacent healthy tissues [3].

## I.4. Radiobiological mechanisms and ROS production

### I.4.1. Pathways of energy deposition: direct vs indirect action

The biological degradation induced by ionizing radiation is fundamentally governed by two primary pathways, distinguished by the site of initial energy deposition.

In direct action, the radiation interacts immediately with the cell's vital targets, predominantly the DNA structure. This mechanism is the hallmark of high-LET radiation, where the dense energy deposition leads to severe and often irreparable lesions.

Conversely, indirect action plays a more pervasive role in clinical radiotherapy using X-rays or gamma rays, accounting for nearly 70% of the total cellular damage. This process is mediated by the interaction of radiation with cellular water molecules, which serves as a precursor to the formation of highly reactive intermediaries [4].

### I.4.2. Kinetics of water radiolysis and radical formation

Given the high aqueous content of biological systems, the radiolysis of water is the most significant source of radiation-induced toxicity. This transformation unfolds across a precise temporal scale, beginning with the physical stage ($10^{-15}$ s) where the initial ionization of ($H_2O$) molecules occurs. This is rapidly followed by the physico-chemical stage, where primary reactive species like the hydroxyl radical ($OH^{\bullet}$) and the hydrated electron ($e^-_{aq}$) emerge. Finally, the chemical stage ($10^{-12}$ to $10^{-6}$ s) allows these radiolytic species to diffuse and interact, leading to the formation of secondary oxidizing agents such as hydrogen peroxide ($H_2O_2$) [5].

### I.4.3. Characterization and reactivity of reactive oxygen species (ROS)

The reactive oxygen species (ROS) generated during irradiation encompass both radical and non-radical molecules, each defined by unique chemical behaviors.

The hydroxyl radical ($OH^{\bullet}$) is recognized as the most lethal species in radiobiology due to its extreme reactivity and extremely short diffusion radius, meaning it attacks biological targets almost at the point of origin.
Other species, such as the superoxide anion ($O_2^{-\cdot}$) and the more stable hydrogen peroxide ($H_2O_2$), contribute to the oxidative onslaught. The transient nature of these species, with half-lives often in the nanosecond range ($10^{-9}$ s), dictates their high probability of reacting with the first biological macromolecule they encounter, thereby limiting their movement but maximizing their local impact [6].

The excessive production of ROS initiates several critical damaging pathways that compromise cellular viability. Lipid peroxidation represents a significant threat, as ROS trigger chain reactions within cell membrane fatty acids, leading to structural loss. Simultaneously, protein oxidation causes the modification of amino acid side chains, resulting in the loss of enzymatic and structural functionality. However, the most critical consequence remains the formation of DNA lesions, ranging from single-strand breaks (SSBs) to lethal double-strand breaks (DSBs). These genomic disruptions are the primary drivers of cell death and the therapeutic effects of radiation [7].

## I.5. Oxidative stress and cellular damage

Oxidative stress is fundamentally characterized as a critical physiological disequilibrium, occurring when the systemic accumulation of reactive oxygen species (ROS) eclipses the inherent neutralizing capacity of the cellular antioxidant defense network. Within the realm of medical physics and radiobiology, ionizing radiation serves as a potent external catalyst that abruptly disrupts this homeostatic balance. By generating an influx of free radicals, radiation shifts the cellular microenvironment into a sustained pro-oxidant state, where the biological system's natural enzymes and molecules can no longer keep pace with the oxidative onslaught [8].

The persistent presence of radiation-induced ROS triggers a cascade of irreversible chemical alterations across essential macromolecules, compromising cellular viability. At the genomic level, DNA damage extends beyond primary strand breaks to include sophisticated base lesions, such as the formation of 8-oxo-7,8-dihydroguanine (8-oxoG). These lesions are particularly hazardous; if they evade the cell's sophisticated repair machinery, they culminate in permanent mutations or the activation of programmed cell death (apoptosis). Simultaneously, the proteome suffers through protein carbonylation, where ROS attack the polypeptide backbone and amino acid side chains. This molecular aggression leads to misfolding and a comprehensive loss of enzymatic functionality. Furthermore, membrane degradation via lipid peroxidation transforms stable membrane lipids into toxic reactive aldehydes, a process that not only destroys membrane integrity but also facilitates the propagation of oxidative damage throughout the cell [9].

Beyond direct structural degradation, oxidative stress significantly interferes with the intricate signaling pathways that maintain cellular homeostasis. High concentrations of ROS can act as secondary messengers that trigger inflammatory responses and alter mitochondrial membrane potential, leading to mitochondrial dysfunction. A critical phenomenon in this context is the "bystander effect," where radiation-induced oxidative signals are transmitted to neighboring, non-irradiated cells. This process expands the scope of radiation injury, as healthy adjacent tissues experience stress and genomic instability, thereby complicating the overall therapeutic ratio in radiotherapy [10].

## I.6. Radioprotection in radiotherapy

The fundamental challenge in radiotherapy resides in the clinical necessity to balance tumor-killing efficiency with the preservation of healthy tissue integrity. Within this context, radioprotection emerges as a critical strategy, encompassing the methodologies and biochemical agents designed to shield non-malignant cells from the deleterious consequences of ionizing radiation. The ultimate goal of these interventions is to optimize the "therapeutic gain" refined ratio that ensures maximum destruction of the oncogenic target while concurrently minimizing the normal tissue complication probability (NTCP). This

requires a sophisticated understanding of how protective agents can selectively intervene in the radiation-induced damage cascade [3].

Radioprotective agents exert their influence through diverse and overlapping biochemical mechanisms aimed at mitigating radiation injury.

A primary pathway involves radical scavenging, where the protector acts as a molecular "buffer" or "sponge," neutralizing highly reactive species such as the hydroxyl radical ($OH^{\bullet}$) before they can initiate irreversible genomic lesions. Furthermore, these agents can facilitate chemical repair by donating hydrogen atoms to damaged biomolecules; this rapid restorative process effectively "fixes" the lesion before it evolves into a permanent structural break. Additionally, some strategies focus on the Modulation of the oxygen effect, reducing local oxygen concentrations in healthy tissues to diminish the overall formation of reactive oxygen species (ROS), thereby enhancing cellular resilience during exposure [4].

Historically, the development of synthetic radioprotectors, such as amifostine, provided a baseline for clinical protection; however, their integration into routine practice has been significantly hindered by systemic toxicity and severe side effects. This limitation has catalyzed a paradigm shift in radiobiological research toward natural radioprotectors. Among these, phenolic acids and specifically caffeic acid have gained prominence. These natural derivatives offer a promising alternative due to their inherently low toxicity and high biocompatibility. Their capacity to counteract oxidative stress through potent antioxidant activities provides a safer, more sustainable framework for protecting biological systems, which serves as the primary motivation for the computational investigation in this study [7].

## I.7. Role of biological antioxidants in medical physics

Antioxidants are considered chemical radioprotectors in medical physics. Their main function is to lessen ionizing radiation's indirect effects. Highly reactive species (ROS) are created when radiation reacts with cellular water (radiolysis). These species are neutralized by biological antioxidants before they have a chance to permanently harm cellular membranes or DNA structures [11]. There are two types of defense:

* **Endogenous defense (enzymatic):** These are the biological "shields" that the cell already has, such Catalase and Superoxide Dismutase (SOD). The amount of these enzymes can be used to assess the tissue's radiosensitivity during radiation therapy.

* **Exogenous defense (dietary):** These comprise exogenous substances such as caffeine. These are investigated in your study as possible supplements to improve the defense of healthy tissues against radiation exposure [12].

The "scavenging" process is an energy and charge transfer event from a physics standpoint:

* **Radical scavenging:** To stabilize the ionized species, the antioxidant molecule donates electrons. Your HOMO and LUMO calculations, which gauge how "easily" a molecule might give up an electron to counteract radiation damage, are useful in this situation

* **Chain-breaking:** Putting an end to the radical propagation's kinetic energy, which causes extensive cellular damage [11].

# I.8. Caffeic acid: molecular structure and radioprotective properties

## I.8.1. Chemical architecture and electron delocalization

Caffeic acid (3,4-dihydroxycinnamic acid) (Fig (I.1)) is a major member of the hydroxycinnamic acid family. Its molecular structure is defined by a phenolic ring with two hydroxyl ($OH^{\bullet}$) groups connected in the ortho position (creating a catechol moiety) and an unsaturated acrylic acid side chain.

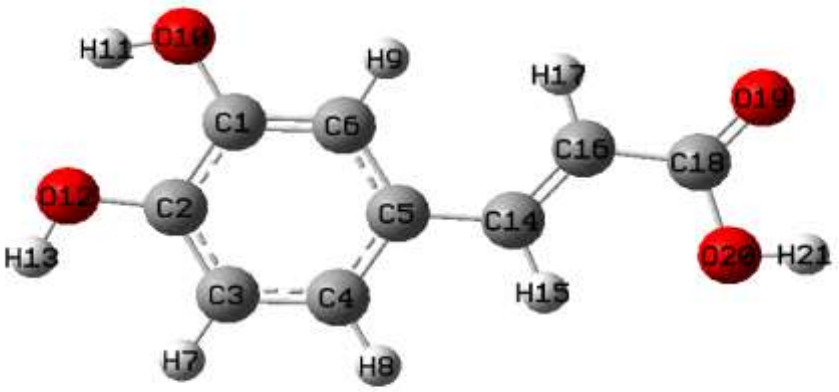


**Figure (I.1):** Optimized structure of caffeic acid at the B3LYP/6-31G(d,p) level of theory.

From a quantum physics perspective, the presence of the double bond in the side chain conjugated with the aromatic ring is important. This unique structure allows for substantial (π-electron) delocalization across the whole molecular frame. When the molecule interacts with a radiation-induced radical, its delocalization helps stabilize the ensuing phenoxyl radical, making caffeic acid an unusually efficient electron donor in the process of neutralizing ionized species [13].

## I.8.2. Biological roles: antioxidant and radioprotector capacity

In biological contexts, caffeic acid acts as a potent scavenger of reactive oxygen species (ROS) such as hydroxyl radicals ($OH^{\bullet}$) and superoxide anions ($O_2^{-\cdot}$), which are the principal damaging products of water radiolysis. Its biological importance in medicinal contexts originates from :

* **High bioavailability:** It is easily absorbed by cellular membranes, allowing it to give interior protection to vulnerable organelles.

* **Synergistic effects:** It has the ability to restore other endogenous antioxidants, hence strengthening the total cellular defense mechanism against radiation-induced oxidative stress [14].

The interest in caffeic acid within radiotherapy research stems in its potential as a "selective radioprotector". Current research reveal that phenolic acids can give a degree of protection to healthy tissues from ionizing radiation damage while retaining the efficacy of the radiation treatment on target tumor cells. This study seeks to further analyze these physical and chemical features using computational models to evaluate the radical scavenging efficacy of caffeic acid, giving a theoretical basis for its usage in clinical radioprotection [14].

Table I.1 lists the various biological sources of Caffeic Acid (CA), correlating their scientific taxonomic names with their common names such as apples, coffee beans, and turmeric [15].

Figure I.2 illustrates the primary biological sources of caffeic acid (CA). Berry fruits, citrus, tea, coffee, olive oil, cocoa, roasted bean, apples, etc., are the main sources of CA [15].

**Table (I.1):** Biological sources of caffeic acid [15]

| Biological Sources | Common Names |
|---|---|
| *Malus domestica* | Apples |
| *Fragaria ananassa* | Strawberries |
| *Brassica oleracea* | Cauliflower |
| *Raphanus sativus* | Radish |
| *Agaricus bisporus* | Mushroom |
| *Brassica oleracea var. sabellica* | Kale |
| *Pyrus communis* | Pears |
| *Olea europaea* | Olive oil |
| *Curcuma longa* | Turmeric |
| *Ocimum basilicum* | Basil |
| *Thymus vulgaris* | Thyme |
| *Origanum vulgare* | Oregano |
| *Brassica oleracea var. capitata* | Cabbage |
| *Salvia officinalis* | Sage |
| *Vitis vinifera* | Grapes |
| *Helianthus annuus* | Sunflower seeds |
| *Myristica fragrans* | Nutmeg |
| *Carum carvi* | Caraway |
| *Cinnamomum verum* | Cinnamon |
| *Coffea Arabica* | Coffee beans |
| *Solanum tuberosum* | Potato |
| *Propolis* | Propolis |
| *Daucus carota subsp. sativus* | Carrot |
| *Zingiber officinale* | Ginger |

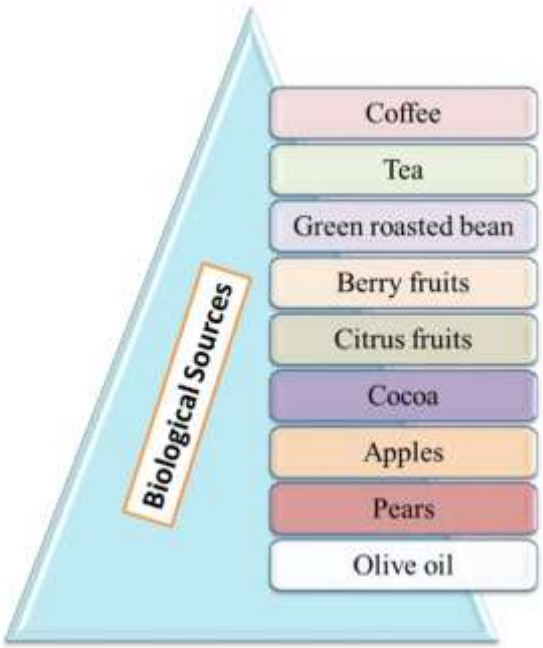


**Figure (I.2):** Common biological sources of caffeic acid [15].

## Conclusion

This chapter demonstrates that understanding the physical basis of the interaction between ionizing radiation and biological matter is fundamental to the development of modern radiotherapy strategies.

We have discussed how radioactive decomposition of water generates reactive oxygen species (ROS), which are the primary cause of oxidative stress and subsequent severe damage to DNA and cellular components.

Caffeic acid also stands out as a promising candidate in radiation protection due to its unique chemical structure, which allows for the delocalization of electrons, granting it a superior ability to neutralize free radicals. This theoretical grounding in the biological and physical mechanisms opens the door to studying the quantum properties of this molecule, which we will explore in the next chapter.

## References

[1] J. G. Webster, and J. D. Bronzino, "Medical instrumentation: Application and Design", 4th ed, Wiley, (2015).

[2] F. H. Attix, "Introduction to Radiological Physics and Radiation Dosimetry", Wiley-VCH, (1986).

[3] F. M. Khan, "The Physics of Radiation Therapy", 5th ed, Lippincott Williams & Wilkins, (2014).

[4] E. J. Hall, and A. J. Giaccia, "Radiobiology for the Radiologist", 8th ed, Lippincott Williams & Wilkins, (2018).

[5] S. Le Caer, Water radiolysis: Influence of the environment on yields and mechanisms, Water, 3, N°1, 235–253, (2011).

[6] P. A. Riley, Free radicals in biology: Oxidative stress and the effects of ionizing radiation, International Journal of Radiation Biology, 65, N°1, 27–33, (1994).

[7] M. C. Joiner, and A. J. van der Kogel, "Basic Clinical Radiobiology", 5th ed, CRC Press, (2018).

[8] H. Sies, Oxidative stress: Oxidants and antioxidants, Experimental Physiology, 82, N°2, 291-295, (1997).

[9] J. Cadet, and J. R. Wagner, DNA base damage by reactive oxygen species, Cold Spring Harbor Perspectives in Biology, 5, N°2, a012559, (2013).

[10] E. I. Azzam, J. P. Jay-Gerin, and D. Pain, Ionizing radiation-induced metabolic oxidative stress and prolonged cell injury, Cancer Letters, 327, N°1-2, 48-60, (2012).

[11] B. Halliwell, and J. M. Gutteridge, "Free Radicals in Biology and Medicine", Oxford University Press, (2015).

[12] R. J. Zampelas, and R. Micha, "Antioxidants in Health and Disease", CRC Press, (2015).

[13] İ. Gülçin, Antioxidant activity of caffeic acid (3, 4-dihydroxycinnamic acid), Toxicology, 217, N°2-3, 213–220, (2006).

[14] C. Magnani, et al., Caffeic acid: A review of its potential as an antioxidant and pharmacologically active molecule, Journal of Food and Nutrition Research, 2, N°11, 770–779, (2014).

[15] Mohd Aijaz, Nishith Keserwani, Mohd Yusuf, Nizamul Haque Ansari, Ruhinaz Ushal, and Pankaj Kalia, "Chemical, Biological, and Pharmacological Prospects of Caffeic Acid", Biointerface Research in Applied Chemistry, Volume 13, Issue 4, 324 (2023).

# CHAPTER TWO: Computational quantum mechanics and DFT

## II.1. Introduction

Quantum chemistry serves as the basic theoretical bridge between fundamental physics and molecular behavior. In the realm of medical physics, it provides the required foundation to understand how possible radioprotectors, such as caffeic acid, respond to the electrical disturbances generated by ionizing radiation at a subatomic level.

## II.2. The quantum mechanical framework

At its root, quantum chemistry is the application of quantum mechanics to molecular systems. Unlike traditional physics, which fails to characterize the behavior of subatomic particles, quantum chemistry treats electrons as wave-functions (ψ). The state of any molecular system is regulated by the Time-Independent Schrödinger Equation: $\hat{H}\psi = E\psi$.

The Hamiltonian operator ($\hat{H}$) represents the overall energy of the system, including the kinetic energy of the electrons and the nuclei, as well as the potential energy coming from electrostatic interactions. For a complex antioxidant like caffeic acid, solving this equation allows for the identification of its most stable electronic configuration and its reactivity toward free radicals [1].

$$\widehat{H} = \widehat{T_n} + \widehat{T_e} + \widehat{V_{ne}} + \widehat{V_{ee}} + \widehat{V_{nn}} \qquad \text{(II-1)}$$

* $\hat{T}_e = -\sum_{i=1}^{N} \frac{1}{2}\nabla_i^2$ : Kinetic energy of the electrons.

* $\hat{T}_n = -\sum_{A=1}^{M} \frac{1}{2M_A}\nabla_A^2$ : Kinetic energy of the nuclei.

* $\hat{V}_{ne} = -\sum_{i=1}^{N}\sum_{A=1}^{M} \frac{Z_A}{r_{iA}}$ : Nucleus-Electron attraction potential.

* $\hat{V}_{ee} = \sum_{i<j}^{N} \frac{1}{r_{ij}}$ : Electron-Electron repulsion potential.

* $\hat{V}_{nn} = \sum_{A<B}^{M} \frac{Z_A Z_B}{R_{AB}}$ : Nucleus-Nucleus repulsion potential.

## II.3. The Born-Oppenheimer approximation

A basic notion in molecular physics is the Born-Oppenheimer approximation. This principle simplifies the many-body issue by assuming that the nuclei, being substantially heavier and slower than electrons, can be considered as stationary points. This permits scientists to focus completely on the electronic Schrödinger equation, which is the key to understanding the process by which caffeic acid transfers electrons to neutralize the extremely reactive species created during the radiolysis of water [1].

$$\widehat{H_{elec}}\Psi_{elec} = E_{elec}\Psi_{elec} \qquad \text{(II -2)}$$

$$\widehat{H_{elec}} = \widehat{T_e} + \widehat{V_{ne}} + \widehat{V_{ee}} + \widehat{V_{nn}} \qquad \text{(II -3)}$$

## II.4. Molecular orbitals and the energy gap

The solution to the electronic equation provides molecular orbitals (MOs), which describe the spatial distribution and energy levels of electrons within the molecule. From a radioprotective perspective, two distinct orbitals are of critical importance:

* **HOMO (highest occupied molecular orbital):** This orbital characterizes the molecule's ability to give electrons (ionization potential).

* **LUMO (lowest unoccupied molecular orbital):** This orbital shows the ability of the molecule to take electrons (electron affinity).

The energy gap ($E_{gap} = E_{LUMO} - E_{HOMO}$) is a crucial physical description. According to recent studies (Abdel-Mottaleb et al.) [2], a smaller energy gap indicates better chemical reactivity and kinetic instability, which are crucial qualities for an efficient antioxidant engaging in rapid charge-transfer activities to stabilize radiation-induced ions.

## II.5. Density functional theory (DFT)

DFT has evolved as one of the most powerful and commonly used computational approaches in molecular physics and quantum chemistry. Its appeal arises from its ability to deliver high-level accuracy in forecasting the electrical characteristics of complicated compounds, such as caffeic acid, with a

substantially reduced computational cost compared to standard wave-function-based approaches

## II.5.1. Fundamental principles: the Hohenberg-Kohn theorems

The physical underpinning of DFT resides in the two Hohenberg-Kohn theorems. These theorems establish that all ground-state features of a multi-electron system are uniquely defined by its electron density ρ(r). This shift in attention from the multi-dimensional wave-function (which depends on *3N* variables for *N* electrons) to the three-dimensional electron density makes it possible to explore the electronic structure of big biological antioxidants more efficiently [3].

$$E[\rho] = T[\rho] + V_{ne}[\rho] + V_{ee}[\rho] \qquad \text{(II -4)}$$

$$E_{DFT}[\rho] = \int \rho(r) v_{ext}(r) dr + F_{HK}[\rho] \qquad \text{(II -5)}$$

$* E[\rho]$ : Total energy functional

$* \rho(r)$ : Electron density at position

$*V_{ext}(r)$ : External potential (Nuclei-Electron interaction)

$*F_{HK}[\rho]$ : Universal Hohenberg-Kohn functional

$* T[\rho]$ : Kinetic energy of the electrons

$*V_{ee}[\rho]$ : Electron-Electron repulsion energy

## II.5.2. The Kohn-Sham approach and exchange-correlation

The practical application of DFT is realized by the Kohn-Sham (KS) equations. The KS approach replaces the complex system of interacting electrons with a simpler system of non-interacting particles traveling in an effective external potential. A fundamental feature of this potential is the exchange-correlation functional ($E_{xc}$), which accounts for the quantum mechanical interactions between electrons.

The main equation: $\left[-\frac{1}{2}\nabla^2 + v_{eff}(r)\right]\phi_i(r) = \epsilon_i \phi_i(r)$ (II -6)

The potential equation: $v_{eff}(r) = v_{ext}(r) + \int \frac{\rho(r')}{|r-r'|} dr' + v_{xc}(r)$ (II -7)

* $\phi_i(r)$ : Kohn-Sham orbitals

*$\epsilon_i$ : Orbital energies

*$v_{eff}(r)$: Effective potential:

*$v_{ext}(r) = -\sum_{A=1}^{M} \frac{Z_A}{|r-R_A|}$ : External potential (Nuclei-Electron)

* $v_{xc}(r) = \frac{\delta E_{xc}[\rho]}{\delta \rho(r)}$: Exchange-correlation potential

* $\rho(r) = \sum_{i=1}^{N} |\phi_i(r)|^2$ : Electron density

In modern research (Kowalska-Baron et al.) [4], functionals such as B3LYP or the more recent M06-2X are applied to attain great precision in computing the thermodynamic and kinetic parameters of radical scavenging reactions.

### II.5.3. Basis sets in computational modeling

To solve the Kohn-Sham equations numerically within the Gaussian software environment, a basis set is necessary. A basis set is a collection of mathematical functions used to approximate the atomic orbitals.
For the research of phenolic acids, standard basis sets like 6-31G(d,p) are widely utilized. These sets include polarization functions that allow for a clearer description of the electron distribution around the oxygen atoms in the hydroxyl groups, which are the key sites of radioprotective activity in caffeic acid [2].

## II.6. Theoretical evaluation of antioxidant efficiency using DFT descriptors

Density functional theory (DFT) is not only a computational tool but a predictive physical framework that allows medical physicists to estimate the radical-scavenging capability of bio-molecules.

By modeling caffeic acid, we may infer particular electrical parameters that determine its ability to attenuate radiation-induced oxidative damage.

## II.6.1. Analysis of frontier molecular orbitals (FMOs)

The interaction between caffeic acid and unstable radicals is essentially governed by the features of its frontier molecular orbitals. Based on quantum chemistry simulations:

* **Highest occupied molecular orbital (HOMO):** This reflects the "electron-source" of the molecule. A higher energy level for the HOMO suggests that caffeic acid can effectively donate electrons to counteract oxidizing species, such as the hydroxyl radicals generated during water radiolysis [2].

* **Lowest unoccupied molecular orbital (LUMO):** This level shows the molecule's electron-accepting capacity [2].

* **Energy gap (ΔE):** Calculated as the difference between $E_{LUMO}$ and $E_{HOMO}$. From a stability perspective, a smaller gap indicates a more chemically reactive species, which is important for a high-performance antioxidant that must react promptly before the radical damages cellular DNA [2].

## II.6.2. Molecular electrostatic potential (MEP) interpretation

The molecular electrostatic potential MEP map offers a visual and quantitative distribution of the electric charge throughout the molecule surface. In medical physics applications, this map is used to pinpoint:

* **Electrophilic Sites:** Potential locations for radical attack.

* **Nucleophilic Sites:** Regions (typically drawn in red near the hydroxyl groups) that are electron-rich and serve as the active sites for scavenging actions [5].

## Conclusion

This chapter demonstrates that computational chemistry, specifically density functional theory (DFT), provides a robust theoretical framework for predicting the electronic properties of biomolecules. By solving the Kuhn-Sham equation, we were able to understand how to define physical descriptors such as molecular boundary orbitals (HOMO and LUMO) and the energy gap, which are direct indicators of a molecule's antioxidant efficacy.

The analysis of these indicators, along with molecular electrostatic potential (MEP) maps, (paves the way for the application in the next chapter), where numerical calculations and computational modeling using gaussian software will be performed to evaluate the actual radiation shielding efficacy of caffeic acid based on these atomic principles.

## References

[1] I. N. Levine, "Quantum Chemistry", 7th ed, Pearson, (2014).

[2] M. S. Abdel-Mottaleb, et al., "DFT Studies of Caffeic Acid Antioxidant: Molecular Orbitals and Composite Reactivity Maps", Journal of Chemistry, 2016, 1–10, (2016).

[3] W. Koch, and M. C. Holthausen, "A Chemist's Guide to Density Functional Theory", 2nd ed, Wiley-VCH, (2015).

[4] A. Kowalska-Baron, Theoretical insight into antioxidant mechanism of caffeic acid, International Journal of Molecular Sciences, 25, N°1, 456, (2024).

[5] A. Masek, et al., Determination of antioxidant activity of caffeic acid, International Journal of Electrochemical Science, 11, 10644–10653, (2016).

# CHAPTER THREE: COMPUTATIONAL AND APPLIED STUDY OF CAFFEIC ACID

# III.1. Introduction

The application of quantitative chemical computation has become an indispensable tool in medical physics and drug design, providing a detailed molecular view that complements experimental results.

Caffeic acid (CA), a prominent phenolic compound, has garnered significant attention for its ability to mitigate oxidative stress induced by ionizing radiation [1]. While the biological activity of these antioxidants is often evaluated in vivo, theoretical modeling using density function theory (DFT) allows for a precise investigation of the electronic properties that govern their radiation-protective capacity.

These computational approaches enable us to identify critical indicators, such as the HOMO and LUMO molecular orbital energies, which are key indicators of chemical reactivity and free radical scavenging activity. Furthermore, molecular electrostatic potential (MEP) and bond dissociation energies (BDE) analysis provide insights into how caffeic acid interacts with reactive oxygen species (ROS) at the subatomic level.

This chapter details the computational methodology employed and discusses the resulting data for caffeic acid, thus establishing a theoretical framework for its potential use as a radiation shielding agent in clinical radiotherapy.

# III.2. Computational details and methodology

## III.2.1 Software used:

The theoretical investigation of the structural and electronic properties of caffeic acid (CA) was performed in both the vacuum phase and the aqueous phase using the Gaussian 16 software package (Fig. III.1) [2]. This specific version was selected for its advanced parallel processing capabilities and refined algorithms, which ensure high-precision convergence in complex Density Functional Theory (DFT) calculations.

To facilitate structural modeling and the visual interpretation of molecular properties, GaussView 6 (Fig.III.2) was utilized as a graphical interface to ensure accurate structural modeling and to facilitate the visual interpretation of molecular orbitals and electrostatic potential maps.

**Figure (III.1):** Gaussian 16 Software Logo

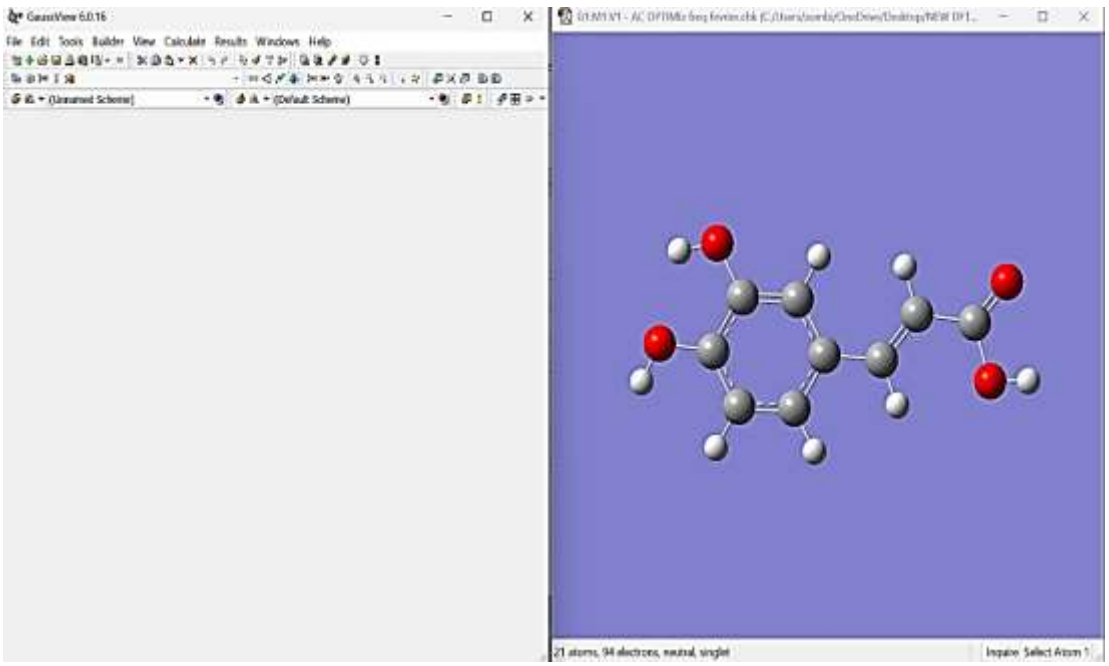

**Figure (III.2):** Visual interface of GaussView showing the optimized molecular structure of caffeic acid.

### III.2.2 Functional and basis set:

Geometry optimization was conducted using the hybrid functional B3LYP. This functional was chosen because it effectively bridges the gap between accuracy and computational cost, providing reliable predictions for the electronic structures and thermochemical data of organic polyphenols [1,3,4].

To achieve a high level of precision, the 6-311G(d,p) triple-zeta basis set was employed, incorporating polarization functions to accurately describe the electron density distribution around both heavy atoms and hydrogens.

Furthermore, the solvent effects of water were simulated using the polarizable continuum model (PCM). This dual-phase approach is essential for understanding how the medium's dielectric constant influences the molecular stability and radical scavenging mechanisms of the compound. All optimized structures were confirmed to be at a local energy minimum through frequency analysis, as indicated by the absence of imaginary frequencies.

## III.3. Geometry optimization

### III.3.1. Geometry optimization of caffeic acid in vacuum and in aqueous phase

In this section, a comprehensive geometric optimization of the molecular structure of caffeic acid was performed to discover its most stable structure in vacuum and in aqueous conditions. The optimization was carried out utilizing the B3LYP functional connected to the 6-311G(d,p) base. To simulate the biological environment.

The following illustration (Fig III.3) provides a visual representation of the energy-minimized geometry for the studied molecules.

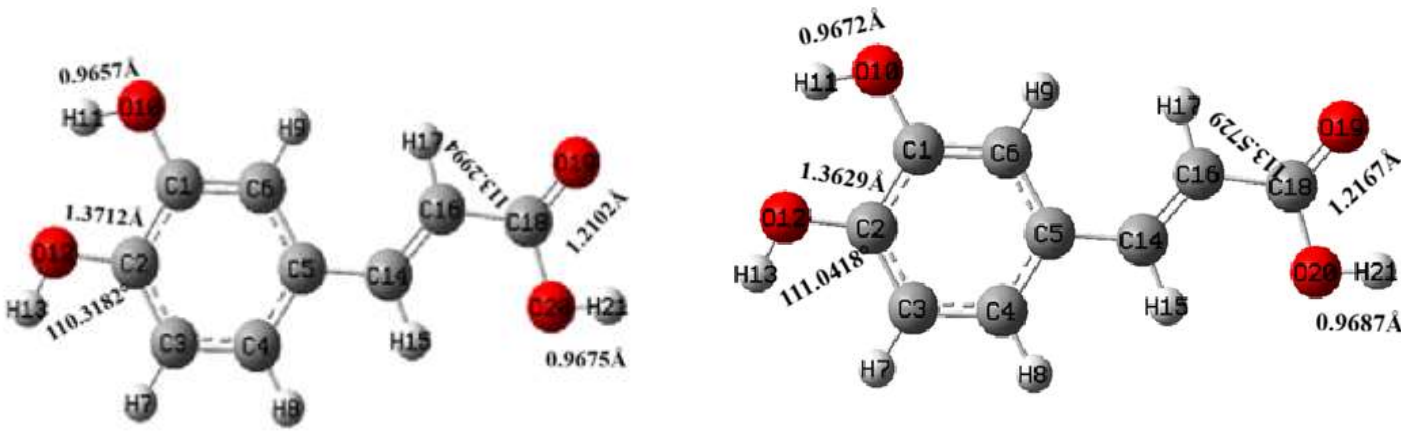


**A** **B**

**Figure (III.3):** Optimized molecular structure and atom numbering of caffeic acid (CA) calculated at the B3LYP/6-311G(d,p) level of theory:

**A**: in vacuum

**B**: in water

As seen in Fig (III.3), the optimal structure of caffeic acid has a typical almost planar shape. This planar configuration is supported by the substantial conjugation between the catechol ring (containing the two neighboring hydroxyl groups, O10-H11 and O12-H13) and the π-system of the propenoic acid side chain (C14=C16). The atom numbering scheme displayed in the figure will be adopted throughout the future examination of bond lengths, angles, and electrochemical properties to ensure clarity and consistency.

Table (III.1) presents the optimized bond lengths of caffeic acid in both the vacuum and aqueous phases, providing a quantitative basis for analyzing the structural adjustments induced by the solvent environment.

**Table (III.1):** Optimized bond lengths (Å) of caffeic acid in the vacuum and aqueous phase calculated at the B3LYP/6-311G(d,p) level of theory .

| Bond | Length (Å) (in the vacuum phase) | Length (Å) (in the aqueous phase) |
|---|---|---|
| C1-C2 | 1.4084 | 1.4113 |
| C1-C6 | 1.3829 | 1.3822 |
| C1-O10 | 1.3597 | 1.362 |
| C2-C3 | 1.3872 | 1.3893 |
| C2-O12 | 1.3712 | 1.3629 |
| C3-C4 | 1.3927 | 1.3927 |
| C3-H7 | 1.0858 | 1.0836 |
| C4-C5 | 1.4017 | 1.403 |
| C4-H8 | 1.0837 | 1.0836 |
| C5-C6 | 1.4076 | 1.4079 |
| C5-C14 | 1.4597 | 1.4571 |
| C6-H9 | 1.0826 | 1.0829 |
| O10-H11 | 0.9657 | 0.9672 |
| O12_H13 | 0.9623 | 0.9645 |
| C14-H15 | 1.0859 | 1.0859 |
| C14-C16 | 1.3440 | 1.3471 |
| C16-H17 | 1.0829 | 1.0830 |

| | | |
|---|---|---|
| C16-C18 | 1.4684 | 1.4649 |
| C18-O19 | 1.2102 | 1.2167 |
| C18-O20 | 1.3627 | 1.356 |
| O20-H21 | 0.9675 | 0.9687 |

The structural change observed in caffeic acid when changing from the vacuum phase to the aqueous phase primarily targets the reactive functional groups of caffeic acid rather than the aromatic skeleton. Under aqueous conditions, the length of the carbonyl group C18–O19 increases to 1.2167Å and the O-H bonds, such as the lengths of O10–H11 and O20–H21, increase to 0.9672Å and 0.9687 Å, respectively.

The expansion of the aforementioned bond lengths, which can be attributed to the polarity of the solvent, significantly reduces the strength of the bonds, which promotes the occurrence of the HAT reaction process. Interestingly, the C2–O12 and C18–O20 bond lengths shorten to 1.3629Å and 1.356Å, respectively. It implies that there is an enhancement in the double bond character in caffeic acid under the presence of the solvent, which suggests that the aqueous phase may promote the delocalization of the charge within the structure. It would provide additional stability to the formed phenoxyl radical, preventing any participation in other chain reactions, which is required in order to achieve antioxidant activity. The C14-C16, known as the vinyl bridge, experiences only a small extension by 0.0032 Å. However, the C3-C4, a carbon-carbon bond within the benzene ring, does not experience any alterations at all.

The calculated bond angles of caffeic acid, as determined at the B3LYP/6-311G(d,p) level of theory, are summarized below (Tab (III.2) and Tab (III.3) to illustrate the conformational reorientations and subtle angular shifts that accompany the transition from a vacuum to an aqueous medium.

**Table (III.2):** Optimized bond angles (°) of caffeic acid in the vacuum and aqueous phase calculated at the B3LYP/6-311G(d,p) level of theory.

| Angle | Value (°) (in the vacuum phase) | Value (°) (in the aqueous phase) |
|---|---|---|
| C2-C1-C6 | 119.6062 | 119.8445 |
| C2-C1-O10 | 120.2845 | 120.1078 |
| C6-C1-O10 | 120.1093 | 120.0477 |
| C1-C2-C3 | 120.2269 | 120.0557 |
| C1-C2-O12 | 114.9162 | 114.8228 |
| C3-C2-O12 | 124.8569 | 125.1215 |
| C2-C3-C4 | 119.7950 | 119.7682 |
| C2-C3-H7 | 119.8296 | 119.7737 |
| C4-C3-H7 | 120.3754 | 120.4581 |
| C3-C4-C5 | 120.9123 | 121.0154 |
| C3-C4-H8 | 119.5224 | 119.3969 |
| C5-C4-H8 | 119.5653 | 119.5877 |
| C4-C5-C6 | 118.5374 | 118.5603 |
| C4-C5-C14 | 118.6101 | 118.5945 |
| C6-C5-C14 | 122.8525 | 122.8452 |
| C1-C6-C5 | 120.9222 | 120.756 |
| C1-C6-H9 | 117.6482 | 117.8809 |

| | | |
|---|---|---|
| C5-C6-H9 | 121.4296 | 121.3631 |
| C1-O10-H11 | 108.0476 | 108.2525 |
| C2-O12-H13 | 110.3182 | 111.0418 |
| C5-C14-H15 | 115.2980 | 115.0899 |
| C5-C14-C16 | 127.4526 | 127.427 |
| H15-C14-C16 | 117.2494 | 117.483 |
| C14-C16-H17 | 122.7792 | 122.4918 |
| C14-C16-C18 | 123.9214 | 123.9353 |
| H17-C16-C18 | 113.2994 | 113.5729 |
| C16-C18-O19 | 124.3096 | 123.9677 |
| C16-C18-O20 | 113.9445 | 114.3238 |
| O19-C18-O20 | 121.7459 | 121.7085 |
| C18-O20-H21 | 105.6753 | 106.9541 |

**Table (III.3):** Optimized quaternary bond angles (°) of caffeic acid in the vacuum and aqueous phase calculated at the B3LYP/6-311G(d,p) level of theory.

| Angle | Value (°) (in the vacuum phase) | Value (°) (in the aqueous phase) |
|---|---|---|
| C6-C1-C2-C3 | 0.0026 | 0.0009 |
| C6-C1-C2-O12 | -179.9862 | -179.9988 |
| O10-C1-C2-C3 | -179.9821 | -179.9978 |
| O10-C1-C2-O12 | 0.0291 | 0.0024 |
| C2-C1-C6-C5 | -0.0067 | -0.0008 |
| C2-C1-C6-H9 | -180.0004 | -179.9992 |
| O10-C1-C6-C5 | 179.9781 | 179.9980 |
| O10-C1-C6-H9 | -0.0157 | -0.0005 |
| C2-C1-O10-H11 | -0.0896 | -0.0082 |
| C6-C1-O10-H11 | 179.9257 | 179.9931 |
| C1-C2-C3-C4 | 0.0041 | 0.0001 |
| C1-C2-C3-H7 | 180.0003 | 179.9996 |
| O12-C2-C3-C4 | 179.9917 | 179.9998 |
| O12-C2-C3-H7 | -0.0122 | -0.0007 |
| C1-C2-O12-H13 | -179.9763 | -179.9945 |
| C3-C2-O12-H13 | 0.0356 | 0.0057 |
| C2-C1-C6-H9 | -0.0068 | -179.9992 |
| O10-C1-C6-C5 | 179.9959 | 179.9980 |
| O10-C1-C6-H9 | 179.9970 | -0.0005 |

| | | |
|---|---|---|
| C2-C1-O10-H11 | -0.0003 | -0.0082 |
| C6-C1-O10-H11 | 0.0028 | 179.9931 |
| C1-C2-C3-C4 | -179.9931 | 0.0001 |
| C1-C2-C3-H7 | -179.9999 | 179.9996 |
| O12-C2-C3-C4 | 0.0042 | 179.9998 |
| O12-C2-C3-H7 | 0.0040 | -0.0007 |
| C1-C2-O12-H13 | 179.9975 | -179.9945 |
| C3-C2-O12-H13 | 179.9997 | 0.0057 |
| C2-C1-C6-H9 | -0.0067 | -179.9992 |
| O10-C1-C6-C5 | -0.0581 | 179.9980 |
| O10-C1-C6-H9 | 179.9339 | -0.0005 |
| C2-C1-O10-H11 | 179.9461 | -0.0082 |
| C6-C1-O10-H11 | -0.0619 | 179.9931 |
| C5-C14-C16-H17 | -0.0003 | -0.0007 |
| C5-C14-C16-C18 | -180.0004 | 179.9996 |
| H15-C14-C16-H17 | 179.9916 | 179.9982 |
| H15-C14-C16-C18 | -0.0085 | -0.0015 |
| C14-C16-C18-O19 | -179.9857 | 180.0000 |
| C14-C16-C18-O20 | 0.0006 | -0.0004 |
| H17-C16-C18-O19 | 0.0142 | 0.0003 |
| H17-C16-C18-O20 | -179.9994 | 180.0000 |
| C16-C18-O20-H21 | 180.0091 | -179.9998 |
| O19-C18-O20-H21 | -0.0041 | -0.0001 |

It can be noted from the analysis of optimized bond angles of caffeic acid (Tab III.2 and Tab III.3) that movement from vacuum to water leads to unique changes in the geometric arrangement of atoms that make the molecule act effectively as an antioxidant; Changes are made within reactive centers: C2–O12–H13 angle goes up from 110.3182° to 111.0418°, and C18–O20–H21 angle is also raised from 105.6753° to 106.9541°.

As a result of such changes that occur under influence of hydrogen bonds between solute and solvent, the steric hindrance decreases allowing HAT (the Hydrogen Atom Transfer) reaction to take place by making antioxidant hydrogen easier for abstraction by radicals. In addition, dihedral angles, for instance, C14–C16–C18–O20 angle that stays around 0.00°, reveal that molecules keep their planar structure in both phases.

Planarity allows maximum orbital overlap and therefore enables electrons to be distributed evenly along π-system of benzene ring and propenoic sidechain once a molecule becomes a radical.

Calculated cartesian coordinates for the optimized structures of caffeic acid in vacuum (Tab (III.4)) and water (Tab (III.5)) show the geometric configuration of the molecule at the B3LYP/6-311G(d,p) level.

**Table (III.4):** Optimized cartesian coordinates (Å) of caffeic acid in the vacuum phase calculated at the B3LYP/6-311G(d,p) level of theory.

| Atom | Element | X (Å) | Y (Å) | Z (Å) |
|---|---|---|---|---|
| 1 | C | -2.148139 | 0.847965 | 0.008856 |
| 2 | C | -2.886558 | -0.351379 | 0.009800 |
| 3 | C | -2.232045 | -1.574447 | 0.008062 |
| 4 | C | -0.839923 | -1.614351 | 0.005461 |
| 5 | C | -0.085652 | -0.432851 | 0.004423 |
| 6 | C | -0.766106 | 0.799369 | 0.006130 |
| 7 | H | -2.807697 | -2.495065 | 0.008800 |
| 8 | H | -0.333169 | -2.572233 | 0.004179 |
| 9 | H | -0.230369 | 1.740064 | 0.005467 |
| 10 | O | -2.788471 | 2.047433 | 0.010923 |
| 11 | H | -3.739404 | 1.878940 | 0.011471 |
| 12 | O | -4.248338 | -0.191316 | 0.012233 |
| 13 | H | -4.685518 | -1.048520 | 0.013123 |
| 14 | C | 1.370575 | -0.533254 | 0.001530 |
| 15 | H | 1.765986 | -1.544620 | 0.001374 |
| 16 | C | 2.259339 | 0.474971 | -0.001067 |
| 17 | H | 1.964061 | 1.516786 | -0.001281 |
| 18 | C | 3.715263 | 0.283934 | -0.003880 |
| 19 | O | 4.521642 | 1.186301 | -0.005978 |
| 20 | O | 4.101594 | -1.022865 | -0.003658 |
| 21 | H | 5.068983 | -1.009458 | -0.005486 |

**Table (III.5):** Optimized cartesian coordinates (Å) of caffeic acid in the aqueous phase calculated at the B3LYP/6-311G(d,p) level of theory.

| Atom | Element | X (Å) | Y (Å) | Z (Å) |
|---|---|---|---|---|
| 1 | C | -2.146009 | 0.846125 | -0.000100 |
| 2 | C | -2.888551 | -0.354043 | -0.000176 |
| 3 | C | -2.232048 | -1.578450 | -0.000128 |
| 4 | C | -0.839850 | -1.616581 | -0.000002 |
| 5 | C | -0.084266 | -0.434393 | 0.000050 |
| 6 | C | -0.764593 | 0.800285 | 0.000003 |
| 7 | H | -2.807310 | -2.498098 | -0.000180 |
| 8 | H | -0.333984 | -2.574904 | 0.000046 |
| 9 | H | -0.226734 | 1.740145 | 0.000073 |
| 10 | O | -2.788511 | 2.047042 | -0.000101 |
| 11 | H | -3.741310 | 1.880844 | -0.000291 |
| 12 | O | -4.241525 | -0.189783 | -0.000300 |
| 13 | H | -4.693782 | -1.041645 | -0.000261 |
| 14 | C | 1.369269 | -0.535774 | 0.000137 |
| 15 | H | 1.760178 | -1.548830 | 0.000378 |
| 16 | C | 2.260389 | 0.474406 | -0.000067 |
| 17 | H | 1.960220 | 1.514953 | -0.000340 |
| 18 | C | 3.712864 | 0.283660 | 0.000050 |
| 19 | O | 4.518253 | 1.195615 | -0.000134 |
| 20 | O | 4.105748 | -1.014171 | 0.000393 |
| 21 | H | 5.074457 | -1.016062 | 0.000444 |

Analysis of the structure of caffeic acid on the theoretical level of B3LYP/6-311G(d,p) shows that the molecule maintains a significant amount of planarity both in vacuum and aqueous media.

As shown from the results of the optimized cartesian coordinates, the Z-axis coordinates of all the atoms do not vary much from zero in both cases, thereby showing that the solvents have no effect on the planarity of the catechol ring; However, comparing the two different media, it is observed that there are changes in the cartesian coordinates in both the X and Y axes, due to the influence of water molecules on the molecule through their dielectric characteristics; this implies that the solvent media can influence the polarity and bonding of the polar groups in the molecule.

These results demonstrate that while the fundamental geometric framework of caffeic acid is robust, the aqueous environment induces minor structural relaxations essential for understanding its behavior in biological systems

## III.3.2. Geometry optimization of caffeic acid radical in the vacuum and in the aqueous phase:

Figure (III.4) illustrates the geometry optimization of the radical of caffeic acid calculated at the B3LYP/6-311G(d,p) level of theory.

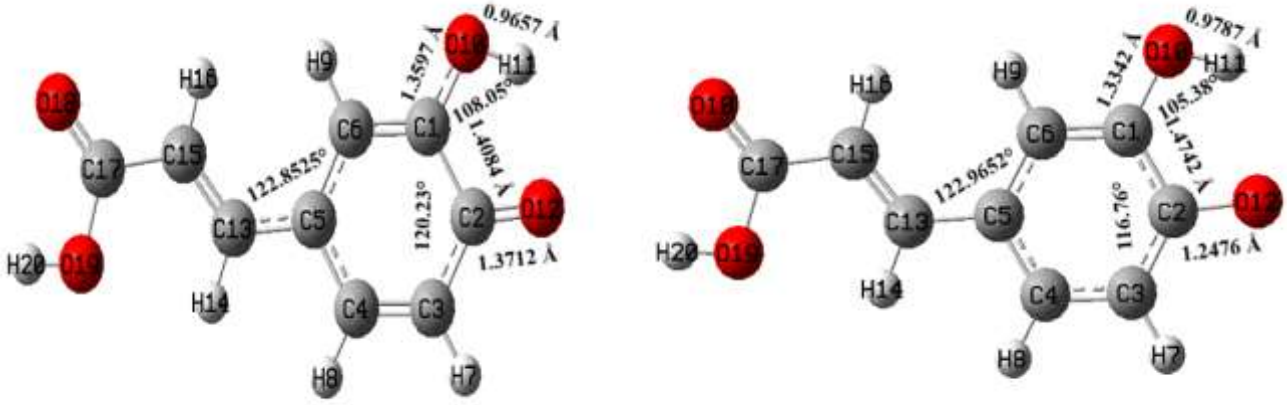


**A** **B**

**Figure (III.4):** Optimized molecular structure and atom numbering of caffeic acid radical (CAR) calculated at the B3LYP/6-311G(d,p) level of theory:

**A** : in vacuum **B**: in water

We observe that the removal of a hydrogen atom from the hydroxyl group at position (O12) does not disrupt molecular symmetry.

The resulting lone electron undergoes extensive delocalization throughout the entire conjugated system (π), enhancing the radical's stability via resonance.

This thermodynamic stability explains the molecule's high capacity to trap free radicals and act as an effective radioprotective agent.

The atomic numbering system shown in the figure will be adopted in all subsequent studies of bond lengths, angles, and electrochemical properties to ensure clarity and consis.

Table (III.6) presents the optimized bond lengths of caffeic acid radical in both the vacuum and aqueous phases, providing a quantitative basis for analyzing the structural adjustments induced by the solvent environment.

**Table (III.6):** Optimized bond lengths (Å) of caffeic acid radical in the vacuum and aqueous phase calculated at the B3LYP/6-311G(d,p) level of theory.

| Bond | Length (Å) (in the vacuum phase) | Length (Å) (in the aqueous phase) |
|---|---|---|
| C1–C2 | 1.4084 | 1.4742 |
| C1–C6 | 1.3829 | 1.3756 |
| C1–O10 | 1.3597 | 1.3342 |
| C2–C3 | 1.3872 | 1.4426 |
| C2–O12 | 1.3712 | 1.2476 |
| C3–C4 | 1.3927 | 1.3634 |
| C3–H7 | 1.0858 | 1.0830 |
| C4–C5 | 1.4017 | 1.4361 |
| C4–H8 | 1.0837 | 1.0840 |

| | | |
|---|---|---|
| C5–C6 | 1.4076 | 1.4099 |
| C5–C13 | 1.4597 | 1.4457 |
| C6–H9 | 1.0826 | 1.0823 |
| O10–H11 | 0.9657 | 0.9787 |
| C13–H14 | 1.0859 | 1.0849 |
| C13–C15 | 1.3440 | 1.3523 |
| C15–H16 | 1.0829 | 1.0825 |
| C15–C17 | 1.4684 | 1.4708 |
| C17–O18 | 1.2102 | 1.2143 |
| C17–O19 | 1.3627 | 1.3511 |
| O19–H20 | 0.9675 | 0.9691 |

The structural analysis of the caffeic acid radical at the B3LYP/6-311G(d,p) level of theory reveals significant geometric reconfigurations when transitioning from the vacuum phase to the aqueous phase.

The most pronounced change is observed in the catechol ring, where the C2–O12 bond undergoes a dramatic contraction from 1.3712 Å in vacuum to 1.2476 Å in water, while the adjacent C1–C2 bond elongates from 1.4084 Å to 1.4742 Å.

Furthermore, the aqueous environment induces an elongation of the O10–H11 hydroxyl bond from 0.9657 Å to 0.9787 Å, alongside a shortening of the C1–O10 bond from 1.3597 Å to 1.3342 Å.

The propenoic side chain exhibits more subtle adjustments, such as the slight contraction of the C5–C13 bond from 1.4597 Å to 1.4457 Å and an increase in the C13–C15 double bond length.

These localized structural relaxations demonstrate that the aqueous phase significantly enhances the polarization and alters the electronic distribution of the radical, which is critical for understanding its antioxidant behavior and chemical reactivity in biological systems [5].

The calculated bond angles of caffeic acid radical, are summarized below (Tab (III.7) and Tab (III.8)), to illustrate the conformational reorientations and subtle angular shifts that accompany the transition from a vacuum to an aqueous medium.

**Table (III.7):** Optimized bond angles (°) of caffeic acid radical in the vacuum and aqueous phase calculated at the B3LYP/6-311G(d,p) level of theory.

| Angle | Value (°) (in the vacuum phase) | Value (°) (in the aqueous phase) |
|---|---|---|
| C2–C1–C6 | 119.6061 | 121.9198 |
| C2–C1–O10 | 120.2846 | 115.6631 |
| C6–C1–O10 | 120.1093 | 122.4171 |
| C1–C2–C3 | 120.2269 | 116.7633 |
| C1–C2–H12 | 114.9162 | 117.8787 |
| C3–C2–H12 | 124.8569 | 125.3580 |
| C2–C3–C4 | 119.7950 | 120.2437 |
| C2–C3–H7 | 119.8296 | 117.8003 |
| C4–C3–H7 | 120.3754 | 121.9560 |
| C3–C4–C5 | 120.9123 | 121.9943 |
| C3–C4–H8 | 119.5224 | 119.9315 |
| C5–C4–H8 | 119.5653 | 118.0742 |
| C4–C5–C6 | 118.5374 | 119.5014 |
| C4–C5–O13 | 118.6100 | 117.5334 |

| | | |
|---|---|---|
| C6–C5–O13 | 122.8525 | 122.9652 |
| C1–C6–C5 | 120.9222 | 119.5775 |
| C1–C6–H9 | 117.6482 | 118.9821 |
| C5–C6–H9 | 121.4296 | 121.4404 |
| C1–O10–H11 | 108.0476 | 105.3795 |
| C5–O13–H14 | 115.2980 | 115.7107 |
| C5–O13–C15 | 127.4525 | 126.6074 |
| H14–O13–C15 | 117.2494 | 117.6818 |
| O13–C15–H16 | 122.7792 | 122.6133 |
| O13–C15–C17 | 123.9214 | 123.8361 |
| H16–C15–C17 | 113.2994 | 113.5507 |
| C15–C17–O18 | 124.3096 | 123.4339 |
| C15–C17–O19 | 113.9446 | 114.0482 |
| O18–C17–O19 | 121.7458 | 122.5179 |
| C17–O19–H20 | 105.6753 | 107.4186 |

**Table (III.8):** Optimized quaternary bond angles (°) of caffeic acid radical in the vacuum and aqueous phase calculated at the B3LYP/6-311G(d,p) level of theory.

| Angle | Value (°) In vacuum phase | Value (°) In aqueous phase |
|---|---|---|
| C6-C1-C2-C3 | 0.0026 | -0.0012 |
| C6-C1-C2-H12 | -179.9861 | 180.0021 |
| O10-C1-C2-C3 | -179.9821 | -180.0003 |
| O10-C1-C2-H12 | 0.0292 | 0.0031 |
| C2-C1-C6-C5 | -0.0067 | 0.0007 |
| C2-C1-C6-H9 | 179.9996 | 180.0017 |
| O10-C1-C6-C5 | 179.9781 | -180.0003 |
| O10-C1-C6-H9 | -0.0156 | 0.0007 |
| C2-C1-O10-H11 | -0.0897 | 0.0001 |
| C6-C1-O10-H11 | 179.9257 | 180.0011 |
| C1-C2-C3-C4 | 0.0041 | 0.0017 |
| C1-C2-C3-H7 | -179.9997 | 180.0011 |
| H12-C2-C3-C4 | 179.9916 | -180.0020 |
| H12-C2-C3-H7 | -0.0122 | -0.0025 |
| C2-C3-C4-C5 | -0.0068 | -0.0016 |
| C2-C3-C4-H8 | 179.9958 | -180.0008 |
| H7-C3-C4-C5 | 179.9971 | -180.0011 |
| H7-C3-C4-H8 | -0.0003 | -0.0003 |

| | | |
|---|---|---|
| C3-C4-C5-C6 | 0.0027 | 0.0011 |
| C3-C4-C5-O13 | -179.9932 | -179.9983 |
| H8-C4-C5-C6 | -179.9999 | -179.9997 |
| H8-C4-C5-O13 | 0.0042 | 0.0009 |
| C4-C5-C6-C1 | 0.0041 | -0.0006 |
| C4-C5-C6-H9 | 179.9975 | 179.9984 |
| O13-C5-C6-C1 | 179.9998 | 179.9988 |
| O13-C5-C6-H9 | -0.0068 | -0.0022 |
| C4-C5-O13-H14 | -0.0582 | -0.0095 |
| C4-C5-O13-C15 | 179.9338 | 179.9890 |
| C6-C5-O13-H14 | 179.9461 | 179.9911 |
| C6-C5-O13-C15 | -0.0619 | -0.0104 |
| C5-O13-C15-H16 | -0.0003 | -0.0007 |
| C5-O13-C15-C17 | 179.9996 | 179.9996 |
| H14-O13-C15-H16 | 179.9916 | 179.9978 |
| H14-O13-C15-C17 | -0.0085 | -0.0019 |
| O13-C15-C17-O18 | -179.9857 | 179.9965 |
| O13-C15-C17-O19 | 0.0006 | 0.0044 |
| H16-C15-C17-O18 | 0.0142 | -0.0033 |
| H16-C15-C17-O19 | -179.9994 | -179.9953 |
| C15-C17-O19-H20 | -179.9908 | 179.9962 |
| O18-C17-O19-H20 | -0.0041 | 0.0041 |

The examination of the bond and quaternary (dihedral) angles for the caffeic acid radical at the B3LYP/6-311G(d,p) level reveals that the aqueous environment affects mostly the angular position of functional groups but not the planarity of the molecule. Some examples include the C1-C2-C3 angle, which shifts from 120.23° in the vacuum state to 116.76° when immersed in an aqueous solution; C2-C1-O10, which decreases from 120.28° in the vacuum state to 115.66° when dissolved in water; and the C1-O10-H11 angle, which contracts from 108.05° in the vacuum state to 105.38° upon solvation.

The above results confirm the solvent effect on molecular relaxation due to its dielectric constant and possible hydrogen-bond formation.

On the other hand, the quaternary angles are still almost 0° or 180° in both cases, with very minor differences (e.g., C6-C1-C2-C3 is near 0°), indicating that the planar conformation of the caffeic acid radical is consistent regardless of the environment.

Therefore, the stability of the conjugation of the caffeic acid radical is well-preserved, while the small difference in bond angles in the aqueous phase reflects the mild electronic attraction and repulsion caused by the solvent.

Tables (III.9) and (III.10) display the arrangement of atoms in cartesian space, offering a very thorough view of the structure of the caffeic acid radical.

**Table (III.9):** Optimized cartesian coordinates (Å) of caffeic acid radical in the vacuum phase calculated at the B3LYP/6-311G(d,p) level of theory.

| Atom | Element | X (Å) | Y (Å) | Z (Å) |
|---|---|---|---|---|
| 1 | C | 2.204804 | 0.820191 | -0.000238 |
| 2 | C | 2.934344 | -0.384575 | 0.000165 |
| 3 | C | 2.270814 | -1.602775 | 0.000376 |
| 4 | C | 0.878432 | -1.632396 | 0.000102 |
| 5 | C | 0.132908 | -0.445356 | -0.000244 |
| 6 | C | 0.822447 | 0.781804 | -0.000368 |

| | | | | |
|---|---|---|---|---|
| 7 | H | 2.839650 | -2.527619 | 0.000691 |
| 8 | H | 0.364616 | -2.586509 | 0.000200 |
| 9 | H | 0.293672 | 1.726430 | -0.000673 |
| 10 | O | 2.853980 | 2.014897 | -0.000811 |
| 11 | H | 3.803642 | 1.839385 | 0.000578 |
| 12 | O | 4.297272 | -0.234573 | 0.000564 |
| 13 | C | -1.324024 | -0.535001 | -0.000368 |
| 14 | H | -1.726894 | -1.543419 | -0.001174 |
| 15 | C | -2.205320 | 0.479761 | 0.000544 |
| 16 | H | -1.902356 | 1.519366 | 0.001518 |
| 17 | C | -3.662618 | 0.299482 | 0.000328 |
| 18 | O | -4.462313 | 1.207781 | 0.000895 |
| 19 | O | -4.058589 | -1.004427 | -0.000881 |
| 20 | H | -5.025855 | -0.983876 | -0.001045 |

**Table (III.10):** Optimized cartesian coordinates (Å) of caffeic acid radical in the aqueous phase calculated at the B3LYP/6-311G(d,p) level of theory.

| Atom | Element | X (Å) | Y (Å) | Z (Å) |
|---|---|---|---|---|
| 1 | C | 2.176374 | 0.857498 | 0.000099 |
| 2 | C | 2.984679 | -0.375308 | 0.000124 |
| 3 | C | 2.263705 | -1.624811 | 0.000059 |
| 4 | C | 0.900326 | -1.630960 | -0.000055 |
| 5 | C | 0.133953 | -0.416457 | -0.000079 |
| 6 | C | 0.801184 | 0.825532 | -0.000006 |
| 7 | H | 2.841064 | -2.541134 | 0.000095 |
| 8 | H | 0.363704 | -2.572785 | -0.000116 |
| 9 | H | 0.254922 | 1.759833 | -0.000048 |
| 10 | O | 2.865252 | 2.000115 | 0.000166 |
| 11 | H | 3.807431 | 1.735173 | 0.000217 |
| 12 | O | 4.226775 | -0.258493 | 0.000263 |
| 13 | C | -1.306851 | -0.535401 | -0.000165 |
| 14 | H | -1.695487 | -1.548285 | -0.000368 |
| 15 | C | -2.199838 | 0.480109 | 0.000008 |
| 16 | H | -1.900374 | 1.520351 | 0.000249 |
| 17 | C | -3.658120 | 0.288365 | -0.000102 |
| 18 | O | -4.453597 | 1.205894 | 0.000118 |
| 19 | O | -4.043164 | -1.006741 | -0.000301 |
| 20 | H | -5.012190 | -1.021303 | -0.000298 |

In the vacuum phase, the geometry of the caffeic acid radical is stable and isolated, where the coordinates on the Z-axis have values close to zero with a slight deviation not exceeding 0.0015 Å.

The coordinates show a balance in the distribution of the aromatic structure, evident in the position of the hydroxyl hydrogen H20, whose value is X = −5.0258, and the radical oxygen O12 has X = 4.2972.

Conversely, in the aqueous phase, the geometry of the molecule is relaxed to adapt to the polarity of the solvent, thus exhibiting a stronger conformability to planarity as the values of the Z-axis approach zero.

The differences in the cartesian coordinates of the radical in the two phases are noticeable, especially those in the catechol ring ; for instance, carbon 2, whose value in the vacuum is X = 2.9343, changes to X = 2.9846 in the aqueous phase. Oxygen 12 in the vacuum environment has X = 4.2972, while in the aqueous environment, the value becomes X = 4.2267.

These spatial adjustments indicate that the aqueous environment induces a more compact and polarized configuration, which is essential for stabilizing the radical through electronic interactions with the surrounding water molecules.

### III.3.3. Summary on structural optimization and comparison between caffeic acid and its radical in vacuum and aqueous phase :

The analytical findings obtained at the B3LYP/6-311G(d,p) level show that the transition of caffeic acid from its neutral to radical state along with the change of medium from vacuum to aqueous is expected to bring about significant modifications in order to optimize the potential of the compound as a radioprotector and antioxidant.

As seen in comparative analysis above, the effect of the solvent on the optimization of the potential is crucial for caffeine acid to function. Throughout all states, the compound maintains a strong planarity since quaternary angles are close to 0° or 180°.

However, due to structural optimization of the compound within the aqueous medium, the relaxation occurs. In the case of the radical state, relaxation

refers to the strong reduction in length of the C2-O12 bond accompanied by increasing length of the O10-H11 bond. The mentioned structural and angular changes (such as the decrease in the angle between the C2-C1-O10 bonds) point to the appearance of the quinonoid configuration along with increasing molecular polarization.

Consequently, the HAT energy barrier decreases; thus, making the molecule a stronger and more stable antioxidant in aqueous media than in vacuum.

## III.4. Energetic results:

After optimizing the structures of the molecules studied using the B3LYP/6-311G(d,p) approach, a thorough energetic evaluation was performed. The above data is crucial for evaluating the stability and electronic properties of the examined systems.

Table (III.11) presents the total electronic energies ($E_{tot}$) of caffeic acid (CA) and its radical (CAR).

The energies are reported in both Hartree and kcal/mol for both the vacuum and the aqueous phase.

**Table (III.11):** Total SCF energies ($E_{tot}$) for CA and CAR in vacuum and aqueous phase calculated at the B3LYP/6-311G(d,p) level of theory.

| Molecular Species | Phase | $E_{tot}$ (Hartree) | $E_{tot}$(Kcal\mol) |
|---|---|---|---|
| Caffeic Acid (CA) | Vacuum | -648.7193 | -407077.2541 |
| | Aqueous | -648.7336 | -407086.175 |
| Caffeic Acid Radical (CAR) | Vacuum | -648.0932 | -406684.3687 |
| | Aqueous | -648.1045 | -406691.4333 |
| Hydrogen atom (H) | both | -0.5002 | -313.9258 |

The energetic data presented in the table reveals a significant difference between the vacuum and the aqueous phase for both caffeic acid (CA) and its radical (CAR).

It is observed that the total energy ($E_{tot}$) in the aqueous phase is lower (more negative) than in the vacuum phase for both species. For example, the energy of Caffeic acid decreases from (-648.7194 Hartree in the vacuum phase to -648.7336 Hartree in the aqueous phase). This decrease indicates that the solvent (water) has a stabilizing effect on the molecules.

This stabilization is due to the solvation effect, where the polar water molecules interact with the hydroxyl and carboxyl groups of caffeic Acid. These interactions lower the potential energy of the system, making the molecule more stable in a biological environment (aqueous medium).

Similarly, the caffeic acid radical (CAR) shows greater stability in water

(-648.1045 Hartree) compared to the vacuum phase (-648.0934 Hartree). This suggests that the aqueous medium facilitates the formation and stabilization of the radical.

The transition from the vacuum phase to the aqueous phase does not change the chemical identity of the molecules but significantly enhances their thermodynamic stability. This confirms that caffeic acid is well-adapted to function as a radioprotector within the aqueous environment of biological cells.

## III.5. Frontier molecular orbitals (HOMO-LUMO) analysis

The electronic properties of caffeic acid (CA) and its radical (CAR) are primarily governed by the frontier molecular orbitals HOMO and LUMO.

The highest occupied molecular orbital (HOMO) acts as an electron donor, its energy level ($E_{HOMO}$) indicates the susceptibility of the molecule to be attacked by electrophiles; Its energy level ($E_{LUMO}$) characterizes the ability of the molecule to gain an electron.

These two orbitals are the main participants in the chemical reactions that occur during the scavenging of reactive oxygen species (ROS).

Table III.12 presents the LUMO and HOMO levels in both vacuum and aqueous phases, allows us to understand how the biological environment influences the antioxidant efficiency of the molecule.

**Table (III.12):** Frontier molecular orbital energies (HOMO, LUMO) for CA and CAR in vacuum and aqueous phase calculated at the B3LYP/6-311G(d,p) level of theory.

| Molecular Species | Phase | $E_{HOMO}$ (eV) | $E_{LUMO}$ (eV) |
|---|---|---|---|
| Caffeic Acid (CA) | Vacuum | -5.87 | -1.64 |
| | Aqueous | -5.83 | -1.76 |
| Radical (CAR) | Vacuum | -5.94 | -2.05 |
| | Aqueous | -5.85 | -1.95 |

The comparison of the frontier molecular orbitals for both caffeic acid (CA) and its radical (CAR) between the vacuum and aqueous phases highlights the significant influence of the solvent:

**For caffeic acid (CA):**

*HOMO level*: In the aqueous phase, the $E_{HOMO}$ increases (from -5.87 eV to -5.83 eV) compared to the vacuum phase. This suggests that water destabilizes the HOMO level slightly, making the molecule more prone to donating electrons to neutralize free radicals in biological environments.

*LUMO Level*: The $E_{LUMO}$ shows a slight stabilization (decrease) in the aqueous phase, which facilitates the redistribution of electronic charges when the molecule interacts with external stressors.

**For the caffeic acid radical (CAR):**

*HOMO Level:* Similar to the neutral acid, the radical's HOMO energy increases in the aqueous phase (moving from -5.94 eV to -5.85 eV). This shift indicates that the solvent environment enhances the radical's electronic profile, which is crucial for its role in the subsequent steps of the antioxidant mechanism.

*LUMO Level*: A notable decrease in $E_{LUMO}$ is observed in the aqueous phase for the radical (from -2.05 eV to -1.95 eV). This stabilization of the LUMO in water reflects the radical's high electron affinity and its readiness to participate in further chemical transformations to stabilize the cellular environment [1].

## III.5.1. Representation of the HOMO and LUMO molecular orbitals of CA

The molecular orbitals were imaged in an aqueous medium (water) using a polarization continuity model (PCM) to simulate biological conditions within the human organism, where water is the primary medium for biological reactions and radiolysis; This study allows for the consideration of polarization and hydrogen bonding effects, making the results more accurate and realistic compared to studies in a vacuum.

Figure.III.5 illustrates the spatial distribution and the electronic density of the HOMO and LUMO orbitals for caffeic acid in an aqueous medium.

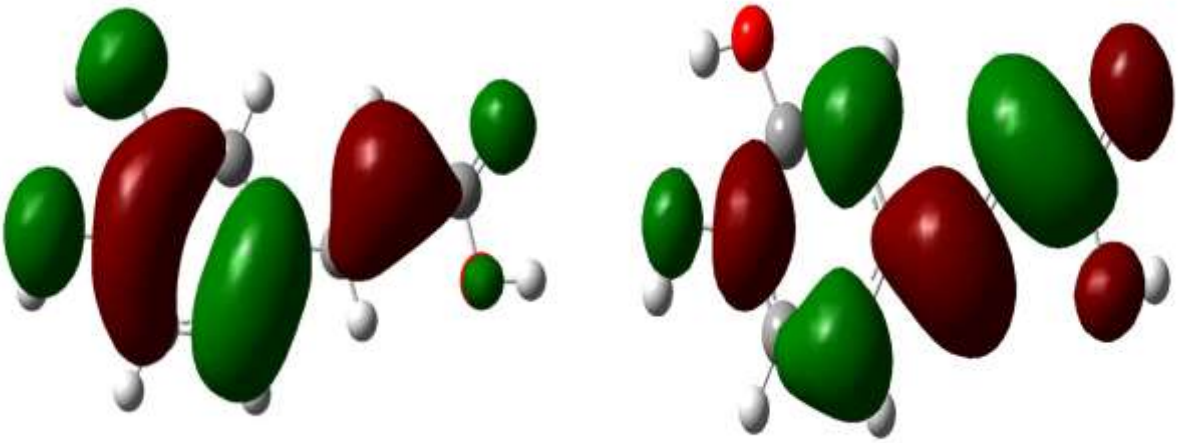

**A** **B**

**Figure (III.5):** 3D visualization of the Frontier Molecular Orbitals (FMOs) for caffeic acid in aqueous phase: (**A**): HOMO orbital (**B**): LUMO orbital.

In the HOMO orbital, we observe that the electron density (red and green clouds) is very concentrated on the benzene ring and the two hydroxyl (OH) groups. This means that these are the "electron-rich" regions, the active sites from which caffeic acid donates electrons to free radicals. This explains its potent antioxidant and radioprotective activity.

In the LUMO orbital, we observe a shift and redistribution of electron density to include the C=C double bond and the carboxyl group (COOH), while remaining on the ring; This indicates the presence of an extended conjugated system in the molecule, which allows for the molecule's stability after electron loss, a process called delocalization.

## III.5.2. Representation of the HOMO and LUMO molecular orbitals of CAR

The following figure (Fig.III.6) displays the frontier molecular orbitals (HOMO and LUMO) of the caffeic acid radical in aqueous phase, highlighting the electronic distribution after the hydrogen atom abstraction:

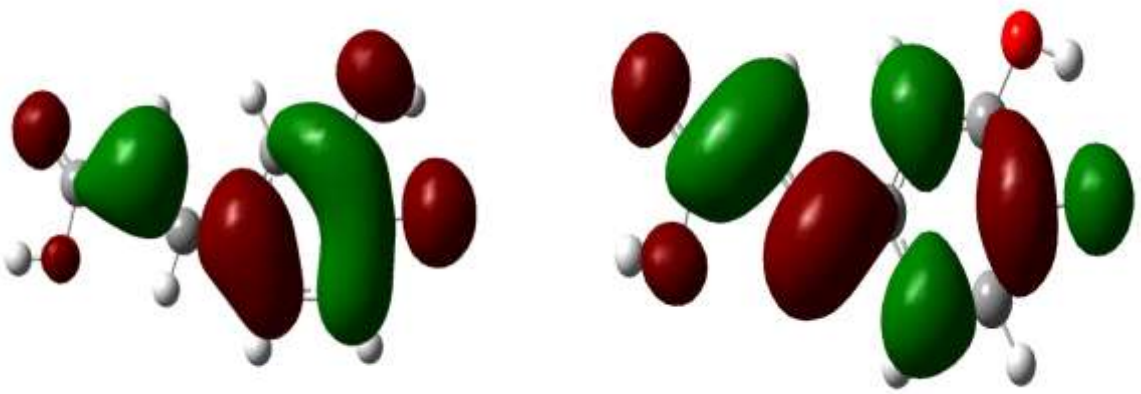

**A** **B**

**Figure (III.6):** 3D visualization of the frontier molecular orbitals (FMOs) for caffeic acid radical in aqueous phase. (**A**): HOMO orbital (**B**): LUMO orbital.

The visualization of the frontier molecular orbitals for the caffeic acid radical provides insight into its stability. As shown in the plot:

*In the HOMO (*A*)*: The electronic cloud is highly concentrated over the oxygen atom that lost the hydrogen and the adjacent carbon atoms of the benzene ring. The red and green lobes indicate that the unpaired electron is not localized on a single atom but is shared across the aromatic system.

*In the LUMO (*B*)*: We observe a further shift and distribution of the lobes across the entire conjugated chain.

This broad distribution of the electronic density (Delocalization) is a key finding. It proves that the Caffeic acid radical is highly stable. In the context of radioprotection, this means that when caffeic acid neutralizes a dangerous radical (like ($OH^{\bullet}$) from water radiolysis), it becomes a stable radical itself, preventing any further "chain reaction" of oxidative damage to biological tissues.

## III.6. Energy gap (ΔE) and chemical reactivity

The energy gap (ΔE), defined as the difference between the LUMO and HOMO energies ($\Delta E = E_{LUMO} - E_{HOMO}$), is a fundamental electronic parameter used to investigate the kinetic stability and chemical reactivity of the studied molecules.

A large energy gap characterizes a "hard" molecule with high kinetic stability, while a small energy gap identifies a "soft" molecule with high chemical reactivity and easier electronic transitions.

The determination of this gap for caffeic acid (CA) and its radical (CAR) in both vacuum and aqueous phases is crucial to understanding the speed and efficiency of the antioxidant process in biological environments.

The calculated values for the energy gap are summarized in the following table (Tab. III.13):

**Table (III.13):** Energy gap (ΔE) for caffeic acid (CA) and its radical (CAR) in vacuum and aqueous phase calculated at the B3LYP/6-311G(d,p) level of theory.

| Molecular Species | Phase | ΔE (eV) | ΔE (kcal/mol) |
|---|---|---|---|
| Caffeic Acid (CA) | Vacuum | 4.23 | 97.548 |
| | Aqueous | 4.07 | 93.858 |
| Radical (CAR) | Vacuum | 3.44 | 79.330 |
| | Aqueous | 3.90 | 89.938 |

A distinct reduction in the energy gap is observed when transitioning from the neutral molecule to its radical form.

In the vacuum phase, the gap decreases from (4.23 eV to 3.44 eV) This indicates that the radical species is kinetically less stable and more chemically reactive ("softer") than the parent molecule.

This high reactivity is a fundamental requirement for an efficient radioprotector, as it ensures the rapid scavenging of free radicals induced by ionizing radiation.

Solvent effect (Vacuum vs. Aqueous Phase): The presence of the aqueous medium has a notable influence on the electronic transition energies: For caffeic acid (CA), the energy gap narrows from (4.23 eV in vacuum to 4.07 eV) in the aqueous phase.

For the radical (CAR), the gap shifts from (3.44 eV to 3.90 eV) The narrowing of the gap in the aqueous phase for the neutral acid suggests that the

polar biological environment facilitates electronic excitation, thereby enhancing the antioxidant efficiency of the molecule in its physiological state.

The calculated ΔE values confirm that caffeic acid possesses a favorable electronic profile for radiation protection.

The lower energy gap in the aqueous medium, compared to the vacuum, implies that the molecule is optimally "activated" within cellular fluids; This allows for more efficient electron transfer processes, which are crucial for neutralizing reactive oxygen species (ROS) and protecting DNA and cellular membranes from oxidative stress.

## III.7. Molecular electrostatic potential (MEP) analysis in aqueous phase.

The MEP calculations for caffeic acid and its radical form were performed exclusively in the aqueous phase using the polarizable continuum model (PCM).

This choice is scientifically justified as caffeic acid primarily exerts its antioxidant and radioprotective activities within biological systems, where water is the dominant solvent.

Studying the molecules in an aqueous environment provides a more realistic representation of its electronic distribution and reactive sites under physiological conditions, accounting for the stabilizing effect of the solvent on polar functional groups and radical species.

### III.7.1. Analysis of MEP for caffeic acid (aqueous phase)

The spatial distribution of the molecular electrostatic potential for caffeic acid in the aqueous phase, where colors visualize the reactive sites is presented in figure.III.7

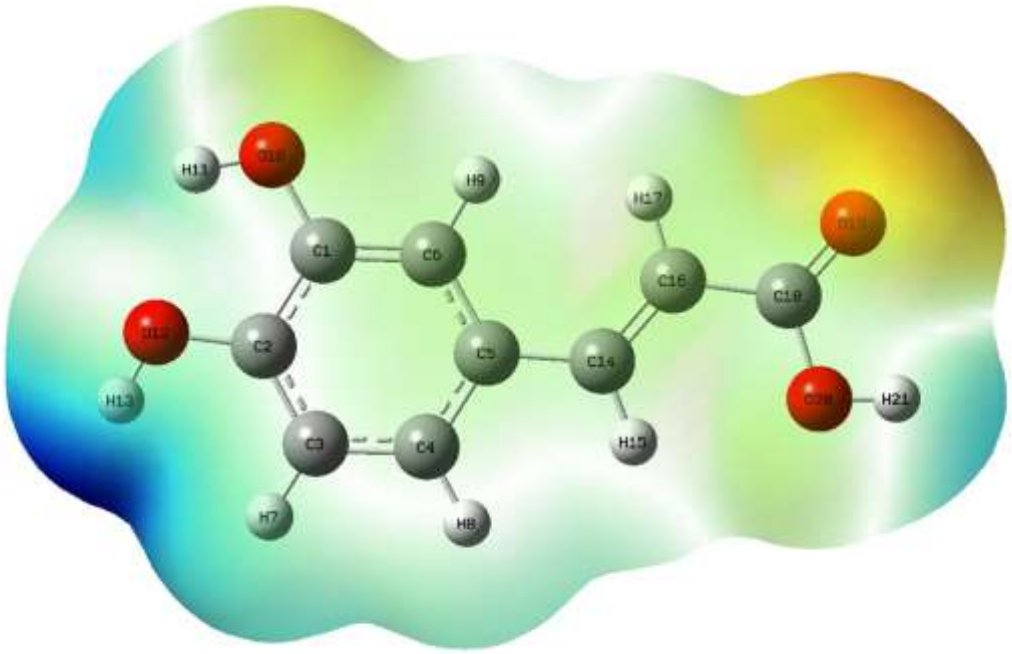


**Figure (III.7)**: Molecular electrostatic potential (MEP) map of caffeic acid calculated in the aqueous phase.

In the neutral molecule, the electrostatic potential is distributed according to standard functional group polarities. In general:

**Electron-rich regions (Red/Orange):** They are concentrated exclusively around the oxygen atoms.

The carbonyl oxygen (O19) of the carboxylic acid group exhibits the most intense red color, indicating the highest negative potential.

Significant negative potential is also localized on the phenolic oxygen atoms (O10and O12).

These sites are the preferred locations for electrophilic attacks.

**Electron-deficient regions (Blue):** They are concentrated on the acidic hydrogen atoms. The most intense blue region is found around the carboxylic hydrogen

(H21), followed by the phenolic hydrogens (H11 and H13), indicating these are the prime sites for nucleophilic interactions.

**Aromatic ring:** The carbon framework of the ring and the side chain appears largely green/light green, indicating near-neutral or slightly negative potential due to the π-conjugated system.

## III.7.2. Analysis of MEP for caffeic acid radical (aqueous phase)

Figure III.8 represents the MEP surface of the Caffeic acid radical in an aqueous environment, highlighting the electronic changes following the hydrogen atom abstraction.

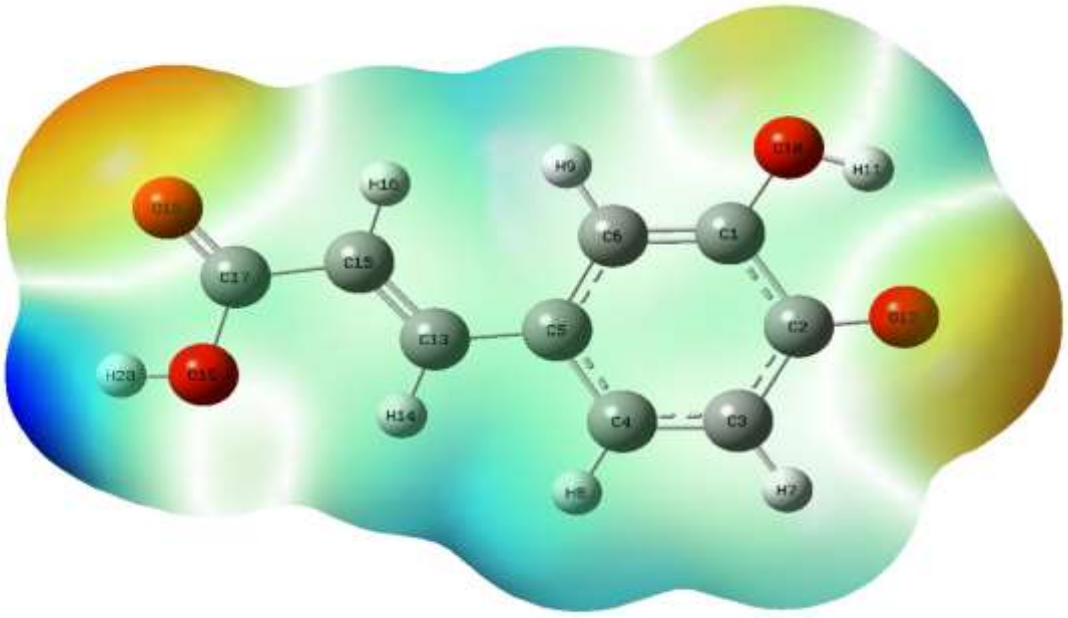


**Figure (III.8):** Molecular electrostatic potential (MEP) map of caffeic acid radical calculated in the aqueous phase.

Upon the formation of the radical (depicted here as loss of hydrogen H13 from the C2-position, forming the deprotonated O12 radical), a massive electronic shift is observed:

**Redistribution of electron density:** The most striking feature is the collapse of the strong negative potential (red) at the carboxylic O18 position. While still

negative (orange), its intensity is significantly reduced compared to the neutral form.

**Shift in reactive sites:** Conversely, the aromatic ring carbon framework, which was nearly neutral in the parent molecule, now exhibits extensive orange and yellow shading (compared to green in Fig.III.7); This shift indicates a substantial (increase in negative potential) across the entire aromatic conjugated system.

**Stabilization by delocalization:** This profound shift directly confirms the delocalization of the unpaired electron's spin density from the specific oxygen atom (O12) across the π-conjugated framework of the aromatic ring. This delocalization stabilizes the radical species by spreading the reactive charge, thus lowering its overall potential energy.

In summary, the transition from caffeic acid to its radical form causes a fundamental rearrangement of the molecule's reactive centers. While the neutral molecule's reactivity is dominated by the strong dipoles of its oxygen-containing functional groups, the radical stability is governed by the ability of the entire conjugated backbone to distribute the unpaired electron density, transforming a previously near-neutral ring into an electron-rich, stabilized system.

## III.8. Bond dissociation enthalpy (BDE) analysis

The bond dissociation enthalpy (BDE) is a key thermodynamic parameter used to evaluate the radical scavenging efficiency of an antioxidant. It represents the energy required for the homolytic cleavage of the O-H bond.

The BDE values were calculated using the total electronic energies ($E_{tot}$) according to the following equation:

$$BDE = E_{tot}(CAR) + E_{tot}(H) - E_{tot}(CA) \quad \text{(III-1)}$$

The calculated total electronic energies for caffeic acid, its radical form, and the atomic hydrogen, along with the resulting bond dissociation enthalpy (BDE) values in both vacuum and aqueous phases, were calculated using are summarized in Table III.14.

**Table (III.14):** Total energies ($E_{tot}$) and calculated BDE values for caffeic acid and its radical in vacuum and aqueous phases.

| Species | $E_{tot}$ (Hartree) | |
|---|---|---|
| | **In vacuum** | **In aqueous phase** |
| **Caffeic Acid (CA)** | -648.7193 | -648.7336 |
| **Caffeic Acid Radical (CAR)** | -648.0932 | -648.1045 |
| **Hydrogen Atom (H)** | -0.5002 | -0.5002 |
| **BDE** | 0.1258 Hartree **(78.96 kcal/mol)** | 0.1287 Hartree **(80.82 kcal/mol)** |

The calculated BDE values provide crucial insights into the radioprotective potential of caffeic acid. The BDE values in both phases **(78.96 kcal/mol and 80.82 kcal/mol)** are relatively low, which is a characteristic of potent antioxidants. This indicates that the (O-H) bond can be easily cleaved to provide a hydrogen atom, effectively scavenging reactive oxygen species (ROS) produced by ionizing radiation.

From a medical physics perspective, this low BDE signifies that caffeic acid can neutralize hydroxyl radicals ($OH^{\bullet}$) generated by water radiolysis before they reach and damage critical cellular components like DNA.

Regarding the solvent effect, a slight increase in the BDE value is observed when moving from the vacuum phase to the aqueous phase. This suggests that the water environment significantly stabilizes the parent caffeic acid molecule through strong solvation and hydrogen bonding, slightly increasing the energy required for deprotonation. Despite this small increase, the BDE remains within an optimal range for biological activity, confirming that caffeic acid is highly efficient in an aqueous cellular environment.

The results obtained for BDE are consistent with the frontier molecular orbital (HOMO-LUMO) analysis.

The ease of hydrogen atom abstraction, combined with the stability of the resulting radical (CAR) through delocalization, proves that caffeic acid is an

excellent candidate for radioprotection in biological systems. This high stability of the radical ensures that the oxidative stress chain reaction is terminated, preventing further damage to tissues.

## III.9. Thermodynamic feasibility of hydroxyl radical ($OH^{\bullet}$) neutralization

To study the efficiency of caffeic acid (CA) in neutralizing hydroxyl radicals ($OH^{\bullet}$) generated by ionizing radiation, we calculated the reaction energy ($\Delta E$); This parameter determines whether the scavenging process is spontaneous and thermodynamically favorable; The reaction follows the following equation:

$$CA + OH \rightarrow CAR + H_2O \qquad \text{(III-2)}$$

The energy reaction is calculated using the following formula:

$$E = [E(CAR) + E(H_2O)] - [E(CA) + E(OH)] \qquad \text{(III-3)}$$

The following table (Tab.III.15) summarizes the calculated energies used and the energy released in the aqueous phase:

**Table (III.15):** Reaction energy ($\Delta E$) for the neutralization of the hydroxyl ion ($OH^{\bullet}$) by caffeic acid in the aqueous phase.

| Species | $E_{tot}$ (Hartree) |
|---|---|
| **Caffeic Acid (CA)** | -648.7336 |
| **Caffeic Acid Radical (CAR)** | -648.1045 |
| **Water ($H_2O$)** | -76.4467 |
| **Hydroxyl Radical (OH)** | -75.7543 |
| **Reaction Energy ($\Delta E$)** | **-0.0633 Hartree (-39.73 kcal/mol)** |

The calculated reaction energy ($\Delta E$) is (-39.73 kcal/mol); The negative value confirms that the neutralization of the hydroxyl radical by caffeic acid is an exothermic process.

In the context of medical physics, this result is of great importance because it demonstrates that caffeic acid is capable of spontaneously neutralizing the highly reactive hydroxyl radical produced during the radiolysis of water.

Since the reaction releases heat ($\Delta E < 0$), caffeic acid acts as an efficient heat sink and chemical shield against oxidative stress. This thermodynamic advantage ensures a rapid protective response, allowing the molecule to protect DNA and cellular structures by converting harmful radicals into stable water molecules before they can cause biological damage. These results strongly support the role of caffeic acid as a potent natural radioprotective agent in aqueous biological environments.

## III.10. Theoretical vibrational frequencies and spectroscopic analysis (FT-IR and Raman).

The vibrational frequencies of neutral and its radical in aqueous phase were calculated at the B3LYP/6-31G(d′,p′) level.

### III.10.1. Spectroscopic analysis for caffeic acid (CA) in aqueous phase:

The computed spectra of neutral caffeic acid in aqueous phase were compared with the experimental [6] IR and Raman data, which is essential to validate the reliability of the theoretical approach (Fig.III.9).

Calculated and experimental spectra show a strong correlation, the agreement confirms the validity of using the B3LYP-D3/6-311+G(d,p) theorem as a reliable approach for characterizing caffeic acid in medical physics research.

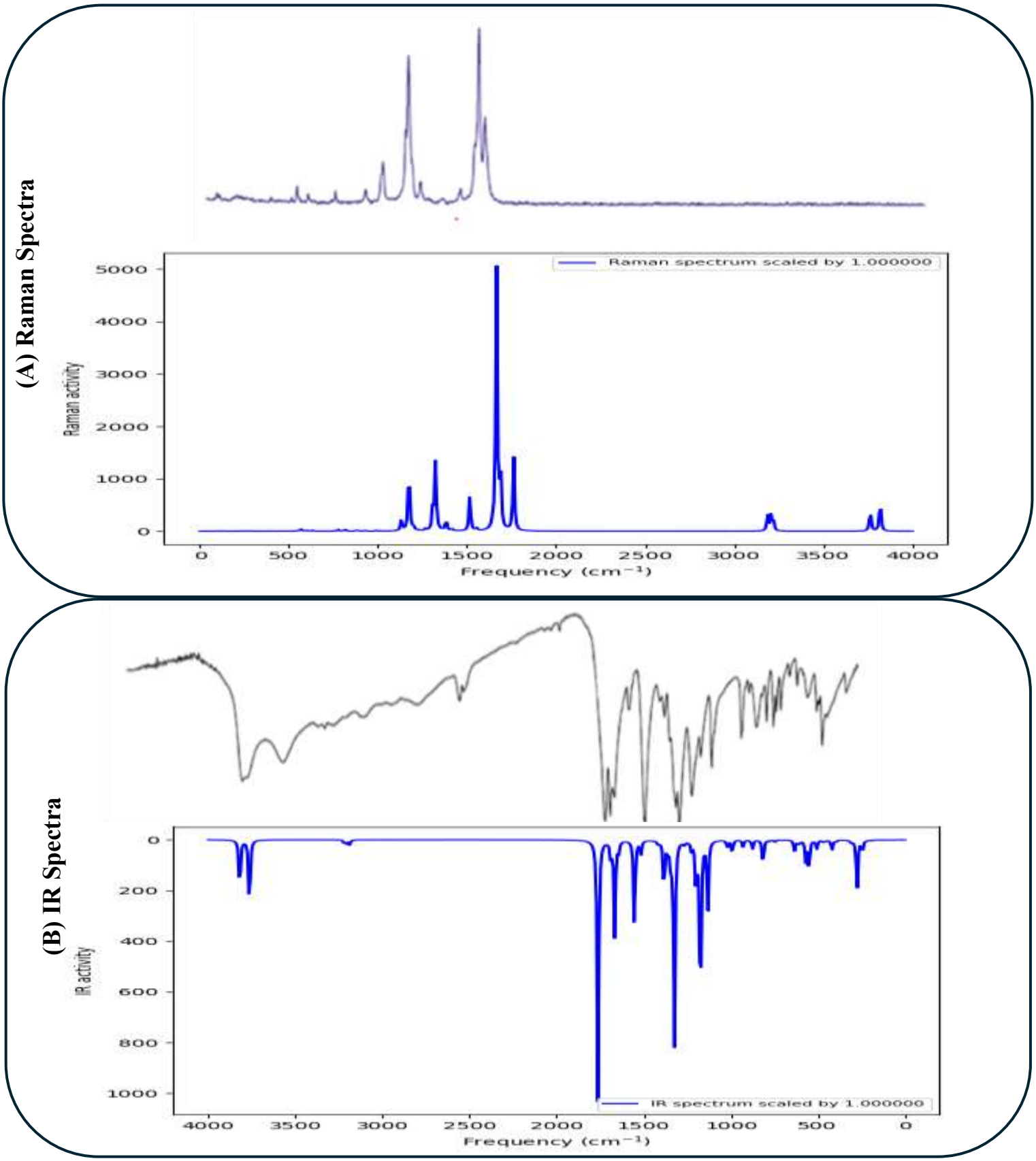


**Figure (III.9):** Experimental [6] (**up**), and **c**alculated (**down**) vibrational spectra of caffeic acid in aqueous solution: (A) Raman spectrum and (B) Infrared (IR) spectrum.

Table **(Annex N° 01 page 77 )** provides a comprehensive comparative analysis of the 57 natural vibrational modes of the studied compound in the aqueous phase; it correlates the theoretical frequencies ($cm^{-1}$) with their measured values and available experimental data [6].

The table also details the spectral response of each mode in both infrared (IR) and Raman spectra, as well as identifying each vibration.

This systematic classification, ranging from low-frequency skeletal vibrations to high-frequency polar bond stretching, allows for a precise understanding of the molecular dynamics and spectral activity in the solvent environment.

The comparison between the calculated vibrational frequencies and the available experimental data [6] for caffeic acid is summarized in the table above. The theoretical frequencies were obtained at the theoretical plane B3LYP-D3/6-311+G(d,p); Based on the results, the following observations can be made:

**High-frequency region (O-H and C-H bond stretching):** The calculated frequencies for the O-H bond stretching modes (modes 55-57) appear in the range of 3763-3820 $cm^{-1}$.

Although the calculations were performed in an aqueous environment, a shift is still observed compared to the experimental values (3231-3550 $cm^{-1}$); This discrepancy is attributed to the fact that the continuum solvent model accounts for the dielectric constant of water but does not fully simulate the specific, discrete intermolecular hydrogen bonds formed in solid or concentrated liquid samples

C-H bond stretching patterns (patterns 50–54) were calculated between 3187 $cm^{-1}$ and 3220 $cm^{-1}$, showing good correlation with the aromatic and non-cyclic CH vibrations.

**Carboxyl and double bond region:** The C=O bond stretching pattern (mode 49) is predicted at 1762.36 $cm^{-1}$, which is consistent with experimental ranges typically observed around 1638–1645 $cm^{-1}$.

This pattern exhibits very high activity in the infrared (1086.10) and Raman (1475.18) spectral signatures, confirming its role as a key spectral signature for caffeic acid.

The C=C bond stretching vibrations (modes 46–48) in the aromatic ring and non-cyclic chain were calculated in the range of 1643–1688 $cm^{-1}$.

Mode 47 exhibits exceptionally high Raman activity (5196.79), indicating a significant change in the molecule's polarization during this vibration.

**Footprint region (C–O and curvature vibration modes):** The C–O stretching vibrations (modes 33–37) lie between 1174 $cm^{-1}$ and 1266 $cm^{-1}$; The high activity in the Raman spectrum of these modes (especially mode 33) reflects the electronic environment of the phenolic hydroxyl groups.

The in-plane and out-plane C–H curvature modes (modes 24–29 and 38–43) show a dense distribution of peaks, characteristic of substituent aromatic systems.

**Low-frequency skeleton vibrations:** Modes 1–23 represent loop skeletal deformations and torsional patterns. These patterns occur at low frequencies between 36 and 777 $cm^{-1}$ and are difficult to detect experimentally, due to their proximity to crystal lattice vibrations and the limitations of standard infrared spectrometers.

The overall agreement between the calculated and experimental spectra indicates that th eB3LYP-D3 method is a reliable option for studying the spectral properties of caffeic acid.

The minor, physically observed deviations are consistent with the omission of intermolecular interactions in the theoretical model.

### III.10.2. Spectroscopic analysis for caffeic acid radical (CAR) in aqueous phase:

To further validate the theoretical results, the calculated Infrared (IR) and Raman spectra of caffeic acid radical are presented in (Fig III.10).

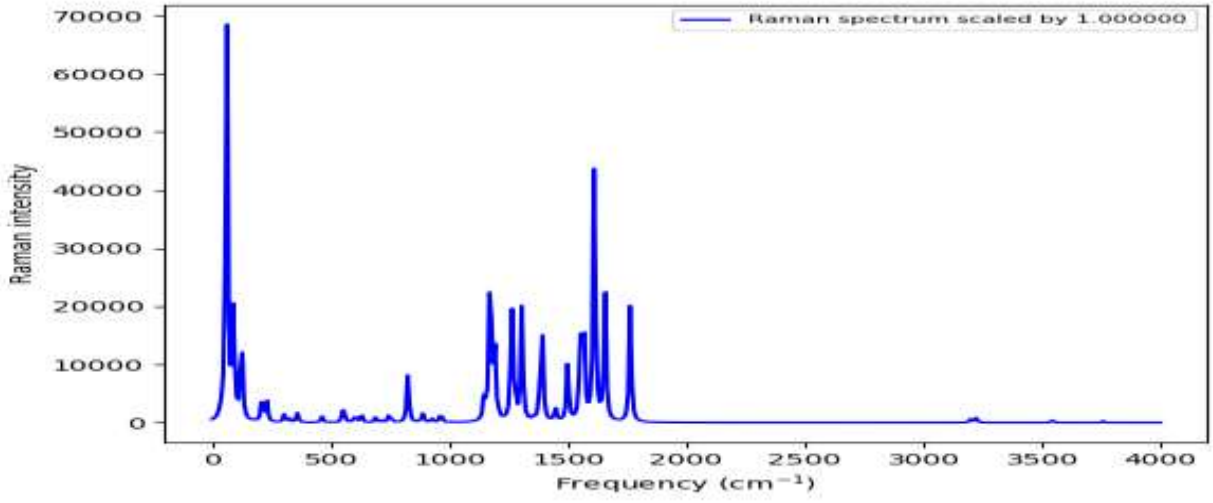


**(A)**

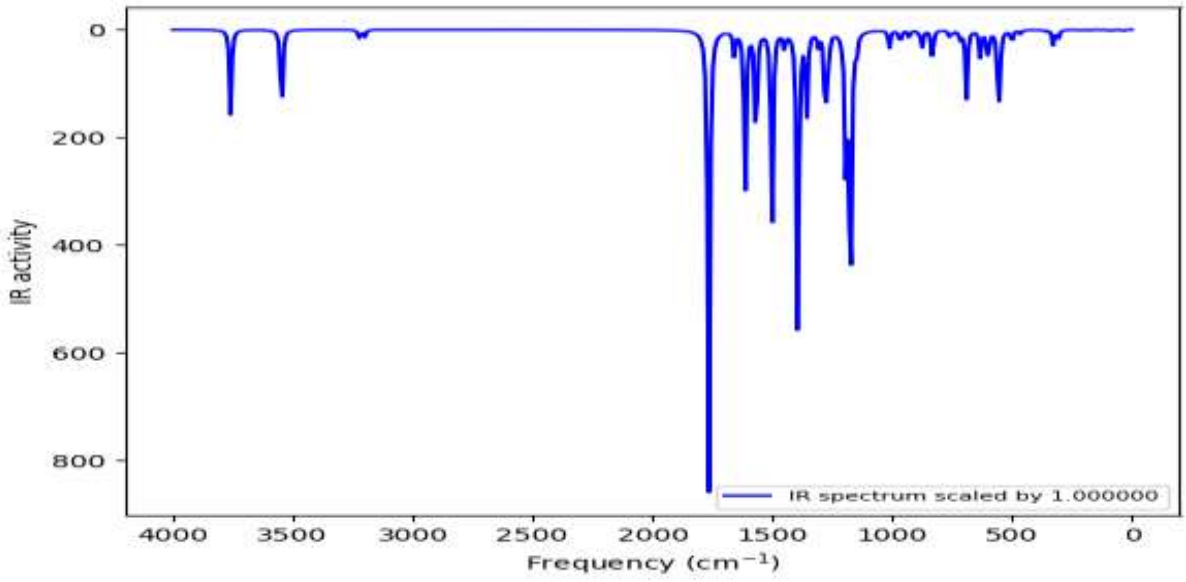


**(B)**

**Figure (III.10):** Calculated vibrational spectra of caffeic acid radical in aqueous solution obtained at the B3LYP-D3/6-311+G(d,p) level of theory:

**(A)** Raman spectrum **(B)** Infrared (IR) spectrum

The calculated Raman and infrared spectra of the caffeic acid radical in aqueous solution show marked changes compared to the neutral form, reflecting a reorganization of the electronic structure following radicalization.

In the Raman spectrum, the redistribution of electron density leads to intense signals in the low-frequency skeleton region and a prominent C=C bond stretching peak near 1600 $cm^{-1}$.

The infrared spectrum is characterized by a dominant C=O bond stretching band at 1764 $cm^{-1}$, confirming the preservation of the carboxyl group.

The C–O bond stretching vibration of the phenoxyl radical at 1173 $cm^{-1}$ is an important spectral indicator for this species, exhibiting high activity in both spectra due to the bond rank change.

These distinctive spectral shifts provide a theoretical "fingerprint" that confirms the stability of the radical and its role as a potential radiation shielding agent in biological environments.

Table **(Annex N° 02 page 81)** presents the calculated vibrational frequencies for the caffeic acid radical. It provides a comparative analysis between infrared (IR) and Raman activities for the 54 normal modes of vibration.

These spectroscopic signatures are essential for identifying the functional groups and structural changes that occur during the radical formation, which directly relates to the antioxidant efficiency and the potential radioprotective properties of the molecule.

Vibrational analysis of the caffeic acid radical reveals several key spectral features that confirm its stability and antioxidant capacity.

The most notable of these is the appearance of a C–O bond stretching pattern at 1173 $cm^{-1}$ (Mode 32), which exhibits the highest activity in both Raman and infrared spectra, making it a definitive spectral indicator of phenoxyl radical formation.

Additionally, mode 40 at 1393 $cm^{-1}$, corresponding to C–C bond stretching in the ring, shows significant activity, reflecting structural modifications within the benzene ring to accommodate the unpaired electron.

The C=C bond stretching at 1612 $cm^{-1}$ and the C=O carboxyl bond stretching at 1764 $cm^{-1}$ also reflect the π-coupling extension of the system. In the high-frequency range, mode 54 at 3758 $cm^{-1}$ represents the O–H bond stretching of the carboxyl group.

Its position and stability indicate that the carboxyl group remains intact and does not directly participate in radical formation, unlike phenolic hydroxyl groups.

This non-localized electron configuration and structural integrity are key factors in the stability of radical species, enhancing the molecule's efficiency in neutralizing free radicals.

In conclusion, the density functional theory (DFT) calculations presented in this study provide an accurate theoretical model of the radical's vibrational profile.

These results confirm that caffeic acid possesses robust structural properties that support its role as an effective biological antioxidant and potential radioprotective agent in medical physics applications, providing a reliable foundation for future spectroscopic research.

Direct comparison with experimental vibrational data for the caffeic acid radical is limited due to its transient nature and extremely short lifetime.

These physical characteristics make the radical highly reactive, presenting significant challenges for isolation and characterization using conventional spectroscopic methods.

Consequently, high-level DFT calculations provide the necessary predictive framework to determine the fundamental spectroscopic properties of this unstable species, which is essential for understanding its behavior in medical physics and antioxidant applications.

## Conclusion

This chapter presents a detailed computational study of the structural, electronic, and thermodynamic properties of caffeic acid (CA) and its radical form (CAR) using density functional theory (DFT) in both vacuum and the aqueous phase.

The results of geometric optimization highlight the molecule's inherent stability, revealing a consistent planar structure that facilitates extensive electron diffusion across the conjugated π system—a crucial feature for radical stability following free radical removal.

Furthermore, the analysis of the HOMO/LUMO boundary molecular orbitals and the resulting energy gap indicates that the aqueous environment enhances the molecule's "chemical flexibility," facilitating electron transfer and making it an ideal candidate for neutralizing hydroxyl radicals (•OH) produced during the radiolysis of water.

Thermodynamic calculations confirm this efficiency, as the low bond dissociation energy (BDE) of approximately 80.82 kcal/mol in water confirms the viability of the hydrogen atom transport (HAT) mechanism, while the negative reaction energy of -39.73 kcal/mol indicates that the process is physically spontaneous and exothermic.

Furthermore, vibrational analysis using Fourier transform infrared (FT-IR) and Raman spectroscopy identified the carbon-oxygen bond vibration at 1173 $cm^{-1}$ as a definitive marker for phenoxyl radical formation, establishing a reliable theoretical criterion for future experimental studies.

Taken together, these computational results demonstrate that caffeic acid acts as a potent chemical shield, capable of intercepting the cascade of oxidative stress reactions before they can damage vital cellular structures such as DNA, thus making it a natural radiation shielding agent in biological systems.

## References

[1] M. S. Abdel-Mottaleb, et al., "DFT Studies of Caffeic Acid Antioxidant: Molecular Orbitals and Composite Reactivity Maps", Journal of Chemistry, 1–10, (2016).

[2] Gaussian 16, Revision C.01, M. J. Frisch, G. W. Trucks, H. B. Schlegel, G. E. Scuseria, M. A. Robb, J. R. Cheeseman, G. Scalmani, V. Barone, G. A. Petersson, H. Nakatsuji, X. Li, M. Caricato, A. V. Marenich, J. Bloino, B. G. Janesko, R. Gomperts, B. Mennucci, H. P. Hratchian, J. V. Ortiz, A. F. Izmaylov, J. L. Sonnenberg, D. Williams-Young, F. Ding, F. Lipparini, F. Egidi, J. Goings, B. Peng, A. Petrone, T. Henderson, D. Ranasinghe, V. G. Zakrzewski, J. Gao, N. Rega, G. Zheng, W. Liang, M. Hada, M. Ehara, K. Toyota, R. Fukuda, J. Hasegawa, M. Ishida, T. Nakajima, Y. Honda, O. Kitao, H. Nakai, T. Vreven, K. Throssell, J. A. Montgomery, Jr., J. E. Peralta, F. Ogliaro, M. J. Bearpark, J. J. Heyd, E. N. Brothers, K. N. Kudin, V. N. Staroverov, T. A. Keith, R. Kobayashi, J. Normand, K. Raghavachari, A. P. Rendell, J. C. Burant, S. S. Iyengar, J. Tomasi, M. Cossi, J. M. Millam, M. Klene, C. Adamo, R. Cammi, J. W. Ochterski, R. L. Martin, K. Morokuma, O. Farkas, J. B. Foresman, and D. J. Fox, Gaussian, Inc., Wallingford CT, 2019.

[3] Leopoldini, M.; Chiodo, S.; Sandro, N.; Toscano, M. Detailed investigation of the OH radical quenching by natural antioxidant caffeic acid studied by quantum mechanical models. J. Chem. Theory Comput *7*, 4218, 2011.

[4] Spiegel, M.; Cel, K.; Sroka, Z. The mechanistic insights into the role of pH and solvent on antiradical and prooxidant properties of polyphenols-nine compounds case study. Food Chem, *407*, 134677. 2023.

[5]M. Lombardo [a], Gustavo Portalone [b], Marcello Colapietro [b], Antonio Rescifin a [a], Francesco Punzo [a] ,Journal of Molecular Structure,Volume 994, 1–3, 2011.

[6] J. Tošović, "SPECTROSCOPIC FEATURES OF CAFFEIC ACID: THEORETICAL STUDY", Kragujevac Journal of Science, Vol. 39, pp. 99-108, (2017)

# General conclusion

# General conclusion

This research presents a comprehensive study of the physical, chemical, and biological properties of caffeic acid as a potential radiation shielding and antioxidant, employing a multidisciplinary approach that integrates medical physics and quantum chemistry.

In the first part of this study, we established a theoretical foundation regarding the nature of ionizing radiation and its interactions with biological materials. The analysis focused on the mechanisms of oxidative stress and the production of reactive oxygen species (ROS) resulting from the radioactive decomposition of water. We highlighted the pivotal role of natural antioxidants, specifically caffeic acid, in neutralizing these harmful free radicals and protecting cellular structures from radiation-induced damage.

The second phase focused on the computational framework, utilizing density functional theory (DFT) to explore the molecular world of caffeic acid. By calculating quantum chemical indices, such as the energy gap between the highest occupied molecular level (HOMO) and the lowest unoccupied molecular level (LUMO), and electronic indices, we gained a deep understanding of the molecule's chemical reactivity and stability at the subatomic level.

Finally, the results obtained confirmed the exceptional efficiency of caffeic acid. Geometric optimization and molecular polarization potential maps revealed the preferred sites for free radical inhibition. The calculated bond dissociation energy, approximately 78.91 kcal/mol (for the most active hydroxyl groups), confirmed its high antioxidant capacity. Furthermore, the electron transport study demonstrated a stable energy gap ($\Delta E$) that explains its reactivity. These theoretical findings were validated by the strong correlation between Fourier transform infrared spectra, calculated Raman spectra, and experimental data.

These results open the door to further studies, including direct simulations of caffeic acid's interaction with complex free radicals, as well as in vitro experiments to match computational results with biological reality. The goal is to improve radiation protection protocols for cancer patients and nuclear and medical personnel.

We hope this modest contribution will be a further building block in the edifice of scientific research aimed at harnessing computational chemistry for the benefit of medical physics and public health.

# ANNEXES

**Annex N° 01**: Calculated vibrational frequencies of caffeic acid in aqueous phase (B3LYP/6-31G(d',p')).

| Mode No. | Calculated frequency ($cm^{-1}$) / Experimental freauency ($cm^{-1}$) [6] | IR Activity | Raman Activity | Assignement |
|---|---|---|---|---|
| 1 | 36.4550 | 0.1961 | 0.0576 | Lattice Vibration |
| 2 | 66.1951 | 1.3514 | 2.1312 | Lattice Vibration |
| 3 | 88.6663 | 0.3767 | 1.4473 | Lattice Vibration |
| 4 | 130.0486 | 1.0513 | 6.1789 | Lattice Vibration |
| 5 | 191.7064 | 2.5811 | 0.4821 | Skeletal Vibration |
| 6 | 212.1282 | 1.8289 | 3.7143 | Skeletal Vibration |
| 7 | 244.1382 | 54.4823 | 8.1412 | Skeletal Vibration |
| 8 | 274.4908 | 215.8011 | 4.7829 | Skeletal Vibration |
| 9 | 306.1065 | 8.8250 | 1.6515 | Torsional Mode |
| 10 | 313.6549 | 3.0458 | 2.8687 | Torsional Mode |

| | | | | |
|---|---|---|---|---|
| 11 | 395.4990 | 8.2563 | 5.7007 | Skeletal Bending |
| 12 | 419.0102 | 45.3932 | 1.7240 | Skeletal Bending |
| 13 | 451.7133 | 2.8383 | 1.8158 | Skeletal Bending |
| 14 | 468.4792<br>470[6] | 11.5673 | 3.1866 | Skeletal Bending |
| 15 | 506.2568<br>520[6] | 36.8825 | 3.6898 | Skeletal Bending |
| 16 | 550.2029<br>560 [6] | 126.4251 | 12.9094 | Skeletal Bending |
| 17 | 569.2508 | 83.4433 | 38.2557 | Skeletal Bending |
| 18 | 598.8902 | 5.3530 | 17.8271 | Ring Deformation |
| 19 | 612.2502<br>600[6] | 18.8732 | 3.4472 | Ring Deformation |
| 20 | 634.7472<br>650[6] | 45.6870 | 16.1770 | Ring Deformation |
| 21 | 709.3538<br>700[6] | 1.0021 | 0.0874 | Skeletal Bending |
| 22 | 746.3975<br>760[6] | 7.8555 | 3.9823 | Skeletal Bending |
| 23 | 777.3728 | 3.7101 | 33.2781 | Skeletal Bending |
| 24 | 813.0555 | 56.1460 | 6.0967 | C-H Out-of-plane |

| | | | | |
|---|---|---|---|---|
| 25 | 816.1607<br>820 [6] | 48.5897 | 31.1548 | C-H Out-of-plane |
| 26 | 875.2113<br>860 [6] | 37.9347 | 8.3668 | C-H Out-of-plane |
| 27 | 886.6737 | 0.3956 | 17.8211 | C-H Out-of-plane |
| 28 | 928.1927<br>910 [6] | 2.7121 | 7.4561 | C-H Out-of-plane |
| 29 | 929.0571 | 24.5674 | 4.2363 | C-H Out-of-plane |
| 30 | 991.2023<br>880 [6] | 53.6172 | 16.4777 | Ring Vibration |
| 31 | 1020.2997<br>1025[6] | 30.7314 | 5.2133 | Ring Breathing |
| 32 | 1132.1278<br>11206] ] | 305.6840 | 218.2922 | C-H Bending |
| 33 | 1174.1662<br>1180[6] | 769.0053 | 1244.1017 | C-O Stretching |
| 34 | 1177.4235 | 18.0354 | 111.5584 | C-O Stretching |
| 35 | 1199.9502 | 189.8279 | 75.6791 | C-O Stretching |
| 36 | 1225.4590 | 35.5231 | 12.5964 | C-O Stretching |
| 37 | 1266.5651 | 12.5706 | 38.8964 | C-O Stretching |
| 38 | 1308.2886 | 3.9243 | 450.4965 | C-H Bending |

| | | | | |
|---|---|---|---|---|
| 39 | 1323.6923 | 843.6158 | 1353.3332 | C-H Bending |
| 40 | 1343.4002 | 111.9060 | 17.9328 | C-H Bending |
| 41 | 1360.8280 | 39.9585 | 12.9576 | C-H Bending |
| 42 | 1383.2187 | 218.0446 | 236.5835 | C-H Bending |
| 43 | 1416.3643 | 14.6005 | 41.9517 | C-H Bending |
| 44 | 1516.4855<br>1515[6] | 56.4053 | 693.4390 | C=C Ring Stretching |
| 45 | 1553.1993 | 368.2023 | 52.6121 | N-H / C=C Bending |
| 46 | 1643.2911<br>1620[6] | 40.6599 | 79.9132 | C=C Stretching |
| 47 | 1666.3265 | 393.6023 | 5196.7930 | C=C Stretching |
| 48 | 1688.6688 | 78.8428 | 1215.0223 | C=C Stretching |
| 49 | 1762.3656<br>1645[6] | 1086.1026 | 1475.1845 | C=O Stretching |
| 50 | 3187.3814<br>3057[6] | 3.0606 | 125.2712 | C-H Stretching |
| 51 | 3188.8573<br>3057[6] | 19.2972 | 216.6085 | C-H Stretching |
| 52 | 3207.1277<br>3057[6] | 14.2907 | 287.4007 | C-H Stretching |

| | | | | |
|---|---|---|---|---|
| 53 | 3212.6699<br>3057[6] | 0.6234 | 16.4595 | C-H Stretching |
| 54 | 3220.4467<br>3057[6] | 13.1415 | 203.2642 | C-H Stretching |
| 55 | 3763.4656<br>3550[6] | 147.9234 | 209.6881 | O-H Stretching |
| 56 | 3764.9315<br>3550[6] | 155.2800 | 218.2736 | O-H Stretching |
| 57 | 3820.0243<br>3550[6] | 220.8790 | 632.7008 | Lattice Vibration |

**Source:** prepared by the student using the program Gaussian 16.

**Annex N° 02 :** Calculated vibrational frequencies, IR Intensities of caffeic acid radical in aqueous phase (B3LYP/6-31G(d',p')).

| Mode No. | Calculated frequency ($cm^{-1}$) | IR Activity | Raman Activity | Assignment |
|---|---|---|---|---|
| 1 | 36.7604 | 2.3983 | 0.02 | Lattice Vibration |
| 2 | 62.6235 | 0.7114 | 5.49 | Lattice Vibration |
| 3 | 90.5476 | 2.3350 | 3.37 | Lattice Vibration |
| 4 | 125.0388 | 0.9153 | 4.80 | Lattice Vibration |
| 5 | 176.5552 | 1.3012 | 0.09 | Skeletal Vibration |
| 6 | 211.6136 | 1.4386 | 04.01 | Skeletal Vibration |
| 7 | 231.6948 | 0.1416 | 3.72 | Skeletal Vibration |

| | | | | |
|---|---|---|---|---|
| 8 | 306.3446 | 16.8907 | 2.90 | Skeletal Vibration |
| 9 | 328.0523 | 28.4787 | 1.23 | Torsional Mode |
| 10 | 360.8397 | 2.5733 | 4.30 | Torsional Mode |
| 11 | 445.2888 | 0.0691 | 0.16 | Skeletal Bending |
| 12 | 464.6393 | 7.1610 | 4.72 | Skeletal Bending |
| 13 | 500.3238 | 24.2117 | 0.53 | Skeletal Bending |
| 14 | 551.6818 | 108.5526 | 11.55 | Skeletal Bending |
| 15 | 558.8749 | 72.3188 | 7.94 | Skeletal Bending |
| 16 | 598.4103 | 50.2004 | 3.76 | Ring Deformation |
| 17 | 606.6808 | 11.9470 | 7.89 | Ring Deformation |
| 18 | 631.5429 | 55.3903 | 11.39 | Ring Deformation |
| 19 | 689.4692 | 127.2388 | 9.43 | Skeletal Bending |
| 20 | 715.4186 | 17.8265 | 4.73 | Skeletal Bending |
| 21 | 748.0088 | 6.4982 | 18.50 | Skeletal Bending |
| 22 | 761.7594 | 10.9755 | 3.70 | Skeletal Bending |
| 23 | 826.6318 | 11.0468 | 136.24 | C-H Out-of-plane |
| 24 | 833.5371 | 43.4598 | 3.17 | C-H Out-of-plane |
| 25 | 875.1203 | 33.5888 | 3.31 | C-H Out-of-plane |

| | | | | |
|---|---|---|---|---|
| 26 | 890.4067 | 3.2204 | 28.69 | C-H Out-of-plane |
| 27 | 928.2585 | 13.4830 | 13.76 | C-H Out-of-plane |
| 28 | 965.7269 | 26.0381 | 39.68 | C-H Out-of-plane |
| 29 | 977.1946 | 1.6759 | 0.43 | Ring Vibration |
| 30 | 1011.2568 | 34.4850 | 2.31 | Ring Breathing |
| 31 | 1148.6714 | 36.5764 | 152.17 | C-H Bending |
| 32 | 1173.6978 | 607.6228 | 1137.92 | C-O Radical site str. |
| 33 | 1192.2629 | 285.2179 | 518.19 | C-H In-plane bending |
| 34 | 1208.2747 | 6.8851 | 29.21 | C-C Stretching |
| 35 | 1264.6003 | 49.7280 | 929.53 | C-O Stretching (Phenolic) |
| 36 | 1278.2556 | 184.4473 | 193.04 | C-H In-plane bending |
| 37 | 1307.3115 | 24.7159 | 945.86 | C-H Bending |
| 38 | 1355.9195 | 159.2083 | 28.63 | C-C Stretching (Ring) |
| 39 | 1383.1683 | 8.9900 | 255.53 | C-H In-plane bending |
| 40 | 1393.1606 | 608.8007 | 865.45 | Ring C-C stretching |
| 41 | 1448.7320 | 32.2465 | 151.04 | C-H Bending |
| 42 | 1500.6394 | 390.6665 | 714.68 | C=C Acyclic stretching |

| | | | | |
|---|---|---|---|---|
| 43 | 1553.3986 | 1.6654 | 982.66 | C=C Ring stretching |
| 44 | 1567.7194 | 239.1362 | 1494.86 | Ring C=C stretching |
| 45 | 1612.7865 | 320.7488 | 3779.96 | C=C Stretching |
| 46 | 1657.9896 | 47.2601 | 1998.35 | C=C Stretching |
| 47 | 1764.3885 | 882.9423 | 2074.64 | C=O Carboxyl str. |
| 48 | 3196.1009 | 1.0717 | 66.51 | Aromatic C-H Stretching |
| 49 | 3198.7266 | 12.1207 | 270.61 | Aromatic C-H Stretching |
| 50 | 3217.0323 | 1.1519 | 3.73 | Alkenyl C-H Stretching |
| 51 | 3220.3291 | 12.9834 | 368.25 | Alkenyl C-H Stretching |
| 52 | 3225.9916 | 5.3873 | 225.75 | Aromatic C-H Stretching |
| 53 | 3546.2433 | 173.2569 | 403.32 | O-H Stretching (Phenolic) |
| 54 | 3758.8003 | 160.6624 | 297.74 | O-H Stretching (Carboxyl) |

**Source**: prepared by the student using the program Gaussian16.

## *ABSTRACT*

***This study evaluates the radioprotective potential of caffeic acid (CA) against ionizing radiation damage using density functional theory (DFT) at the B3LYP/6-311G(d,p) theoretical level. The computational simulation demonstrates that the aqueous phase significantly enhances the molecule's chemical reactivity and structural stability. Through the analysis of HOMO/LUMO orbitals and thermodynamic parameters (BDE, ΔE), the findings reveal that CA exhibits a high electron-donating capacity, enabling it to spontaneously neutralize hydroxyl radicals (OH˙) via the hydrogen atom transfer (HAT) mechanism. Ultimately, these results provide a solid theoretical foundation for utilizing caffeic acid as an effective natural radioprotective agent to mitigate oxidative stress and preserve cellular DNA during clinical radiotherapy.***


**Key words: Caffeic acid, radical, radioprotective, DFT, BDE**


## الملخص

**درسنا خلال هذا البحث الإمكانيات الوقائية الإشعاعية لحمض الكافييك (CA) ضد الأضرار الناجمة عن الإشعاع المؤين، وذلك باستخدام نظرية دالية الكثافة DFT عند المستوى النظري الهجين-B3LYP/6 311G(d,p). وتُظهر المحاكاة الحسابية أن الوسط المائي يعزز بشكل كبير الاستقرار البنيوي والنشاط الكيميائي للجزيء. ومن خلال تحليل المدارات الجزيئية HOMO/LUMO والمعاملات التيرموديناميكية BDE وΔE ، كشفت النتائج أن حمض الكافييك يمتلك قدرة عالية على منح الإلكترونات، مما يمكنه من تعديل جذور الهيدروكسيل الحرة تلقائيًا عبر آلية انتقال ذرة الهيدروجين( HAT) وبالتالي توفر هذه النتائج أساسًا نظريًا صلبًا لاعتماد حمض الكافييك كعامل طبيعي فعال للوقاية الإشعاعية، بهدف تخفيف الإجهاد التأكسدي وحماية الحمض النووي الخلوي DNA أثناء العلاج الإشعاعي السريري.**


**الكلمات المفتاحية: حمض الكافيك ، جذر حر، نظرية دالية الكثافة ، واقٍ من الإشعاع، طاقة تفكك رابطة.**